1st CNS International Summer School
Wako
August 19-23, 2002

Nuclear Shell Model
- Past, Present and Future -

Takaharu Otsuka
Dept. Physics and CNS, Univeristy of Tokyo
RIKEN

M. Honma	Univ. Aizu
T. Mizusaki	Senshu Univ.
Y. Utsuno	JAERI
N. Shimizu	RIKEN
B.A. Brown	MSU
R. Fujimoto	Univ. Tokyo
T. Suzuki	Nihon Univ.

Nuclear Shell Model

- Past, Present and Future -

Outline

I. Basics of shell model calculations

Development of the shell model
Practical Calculations
Dimension Problem
Monte Carlo Shell Model

II. Shell Evolution

Normal vs. Intruder states at N=20
Varying Shell Structure
Spin-Isospin Interaction
Neutron-rich Na isotopes and N=20 gap
^{34}Mg and N=20 gap
pf shell and N=34
p shell and N=6

Shell Evolution Paradigm

Development of the Nuclear Shell Model

Pre-historic age

nucleus = chaos

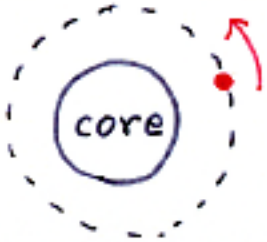

1949 Shell Model proposed by Mayer & Jensen

Single-particle model

orbital motion

Magic numbers , LS splitting

~1960 Core polarization

by Arima & Horie ,

Bohr & Mottelson

||

⇨ Effective Interaction

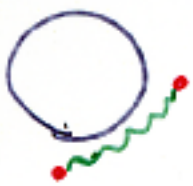

G-matrix : Kuo-Brown, ...

+ new developments (low-k, χPT

Many-body Theory

~1980 sd shell (USD int.)

~1990 "Large-scale" calc.

≳ 1 million dim.

International Conference
Heidelberg
Germany
3-5 June 1999

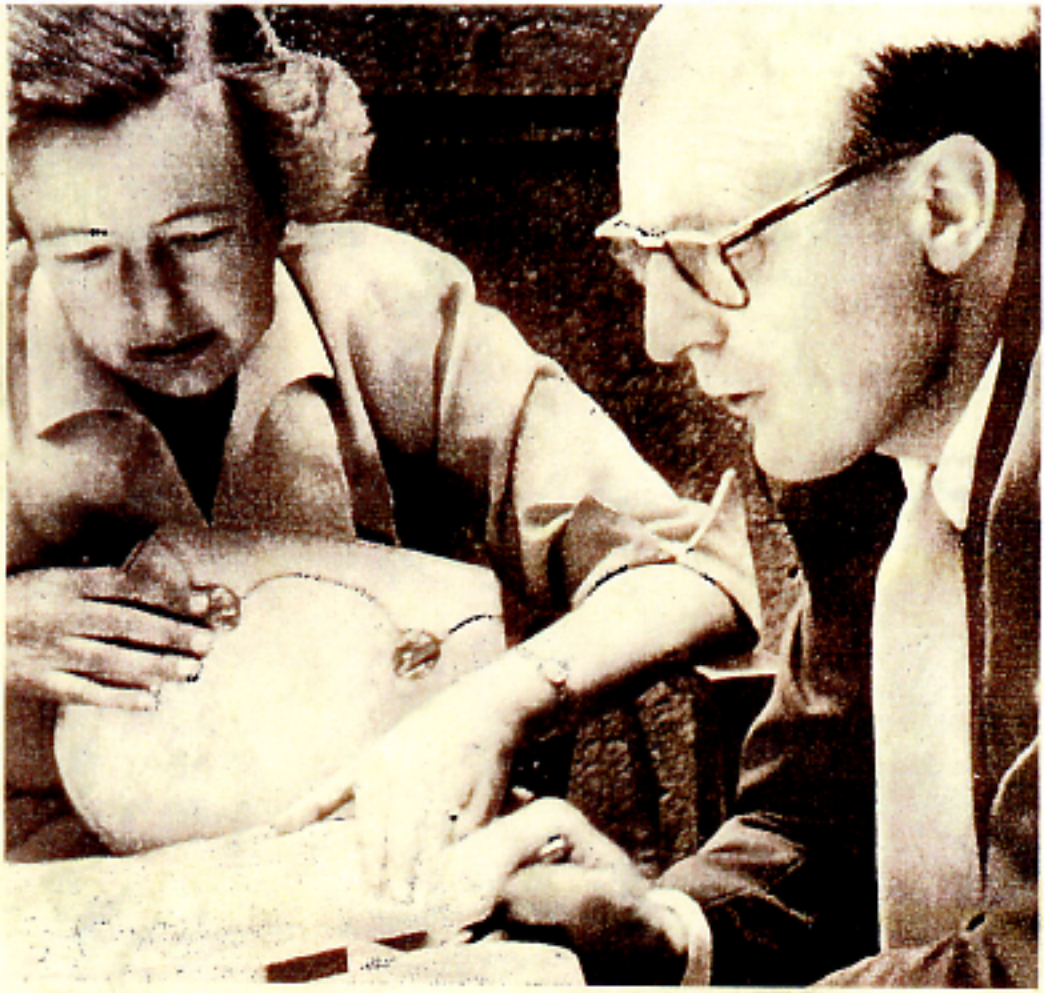

FIFTY YEARS

NUCLEAR SHELL MODEL

PRESENT STATUS AND FUTURE TRENDS

In 1999, fifty years will have passed since Goeppert-Mayer and Haxel, Jensen, and Suess showed that a spin-orbit force can account for the magic numbers in nuclei. This initial discovery paved the way to a detailed understanding of the structure of nuclei in the years that followed. This conference, to be held at one of the birth places of the nuclear shell model (the photograph from the fifties shows Goeppert-Mayer and Jensen at work in Heidelberg), is intended to present a critical review of various aspects of nuclear structure physics, to emphasize open questions and to define directions for further experimental work. The list of speakers includes:

Confirmed Speakers:

S. Aberg (Lund)
G. Bertsch (Seattle)
B. Haas (Strasbourg)
D. Habs (München)
G. Hansen (Michigan)
F. Iachello (New Haven)
S. Mcgrayne (Seattle)
B. Mottelson (Copenhagen)
T. Otsuka (Tokyo)
V. Pandharipande (Urbana)
A. Poves (Madrid)
P. Ring (München)
I. Sick (Basel)
B. Stech (Heidelberg)
H. Weidenmüller (Heidelberg)
D. Wilkinson (Eastbourne)

Advisory Committee:

A. Richter (Darmstadt)
D. Schwalm (Heidelberg)
H. Specht (Darmstadt / Heidelberg)
I. Talmi (Rehovot)

Everyone who is interested in participating is invited to register directly via the homepage (http://frodo.tphys.uni-heidelberg.de/shell99.html) of the conference or to contact the organizers:

Jörg Hüfner
Institute for Theoretical Physics
University of Heidelberg
Philosophenweg 19
D-69120 Heidelberg,Germany
phone: +49-6221-549 440 (secr.:-431,fax:-331)
joerg.huefner@urz.uni-heidelberg.de

Hans A. Weidenmüller
Max-Planck-Institut for Nuclear Physics
Postfach 10 39 80
D-69029 Heidelberg
Germany
phone:+49-6221-516 291 (secr.:-410,fax:-605)
hans.weidenmueller@mpi-hd.mpg.de

Nuclear Shell Model

Mayer

1949

On Closed Shells in Nuclei. II

MARIA GOEPPERT MAYER
Argonne National Laboratory and Department of Physics, University of Chicago, Chicago, Illinois

February 4, 1949

THE spins and magnetic moments of the even-odd nuclei have been used by Feenberg[1,2] and Nordheim[3] to determine the angular momentum of the eigenfunction of the odd particle. The tabulations given by them indicate that spin orbit coupling favors the state of higher total angular momentum. If strong spin-orbit coupling, increasing with angular momentum, is assumed, a level assignment different from either Feenberg or Nordheim is obtained. This assignment encounters a very few contradictions with experimental facts and requires no major crossing of the levels from those of a square well potential. The magic numbers 50, 82, and 126 occur at the place of the spin-orbit splitting of levels of high angular momentum.

Table I contains in column two, in order of decreasing binding energy, the levels of the square well potential. The quantum number gives the number of radial nodes. Two levels of the same quantum number cannot cross for any type of potential well, except due to spin-orbit splitting. No evidence of any crossing is found. Column three contains the usual spectroscopic designation of the levels, as used by Nordheim and Feenberg. Column one groups together those levels which are degenerate for a three-dimensional isotropic oscillator potential. A well with rounded corners will have a behavior in between these two potentials. The shell grouping is given in column five, with the numbers of particles per shell and the total number of particles up to and including each shell in column six and seven, respectively.

Within each shell the levels may be expected to be close in energy, and not necessarily in the order of the table, although the order of levels of the same orbital angular momentum and different spin should be maintained. Two exceptions, $_{11}Na^{23}$ with spin 3/2 in stead of the expected $d_{5/2}$, and $_{25}Mn^{55}$ with 5/2 instead of the expected $f_{7/2}$, are the only violations.

Table II lists the known spins and orbital assignments from magnetic moments[4] when these are known and unambiguous, for the even-odd nuclei up to 83. Beyond 83 the data is limited and no exceptions to the assignment appear.

Up to Z or $N=20$, the assignment is the same as that of Feenberg and Nordheim. At the beginning of the next shell, $f_{7/2}$ levels occur at 21 and 23, as they should. At 28 the $f_{7/2}$ levels should be filled, and no spins of 7/2 are encountered any more in this shell. This subshell may contribute to the stability of Ca^{48}. If the $g_{9/2}$ level did not cross the $p_{1/2}$ or $f_{5/2}$ levels, the first spin of 9/2 should occur at 41, which is indeed the case. Three nuclei with N or $Z=49$ have $g_{9/2}$ orbits. No s or d levels should occur in this shell and there is no evidence for any.

The only exception to the proposed assignment in this shell is the spin 5/2 instead of 7/2 for Mn^{55}, and the fact that the magnetic moment of $_{27}Co^{59}$ indicates a $g_{7/2}$ orbit instead of the expected $f_{7/2}$.

In the next shell two exceptions to the assignment occur. The spin of 1/2 for Mo^{95} with 53 would be a violation, but is experimentally doubtful. The magnetic moment of Eu^{151} indicates $f_{5/2}$ instead of the predicted $d_{5/2}$. No $h_{11/2}$ levels appear. It seems that these levels are filled in pairs only,

TABLE I.

Osc. No.	Square well	Spect. term	Spin term	No. of states	Shells	Total No.
0	$1s$	$1s$	$1s_{1/2}$	2	2	2
			$1p_{3/2}$	4		
1	$1p$	$2p$	$1p_{1/2}$	2	6	8
	$1d$	$3d$	$1d_{5/2}$	6		
2			$1d_{3/2}$	4	12	
	$2s$	$2s$	$2s_{1/2}$	2		20
	$1f$	$4f$	$1f_{7/2}$	8	8?	28?
3			$1f_{5/2}$	6		
	$2p$	$3p$	$2p_{3/2}$	4	22	
			$2p_{1/2}$	2		
			$1g_{9/2}$	10		50
	$1g$	$5g$	$1g_{7/2}$	8		
4			$2d_{5/2}$	6		
	$2d$	$4d$	$2d_{3/2}$	4	32	
	$3s$	$3s$	$3s_{1/2}$	2		
			$1h_{11/2}$	12		82
	$1h$	$6h$				
			$1h_{9/2}$	10		
5			$2f_{7/2}$	8		
	$2f$	$5f$	$2f_{5/2}$	6		
			$3p_{3/2}$	4	44	
	$3p$	$4p$	$3p_{1/2}$	2		
			$1i_{13/2}$	14		126
	$1i$	$7i$				
			$1i_{11/2}$			
6	$2g$	$6g$				
	$3d$	$5d$				
	$4s$	$4s$				

nuclear shell model

Jensen

1949

On the "Magic Numbers" in Nuclear Structure

OTTO HAXEL
Max Planck Institut, Göttingen
J. HANS D. JENSEN
Institut f. theor. Physik, Heidelberg
AND
HANS E. SUESS
Inst. f. phys. Chemie, Hamburg
April 18, 1949

A SIMPLE explanation of the "magic numbers" 14, 28, 50, 82, 126 follows at once from the oscillator model of the nucleus,[1] if one assumes that the spin-orbit coupling in the Yukawa field theory of nuclear forces leads to a strong splitting of a term with angular momentum l into two distinct terms $j=l\pm\frac{1}{2}$.

If, as a first approximation, one describes the field potential of the nucleons already present, acting on the last one added, as that due to an isotropic oscillator; then the energy levels are characterized by a single quantum number $r=r_1+r_2+r_3$, where r_1, r_2, r_3 are the quantum numbers of the oscillator in 3 orthogonal directions. Table I, column 2 shows the multiplicity of a term with a given value of r, column 3 the sum of all multiplicities up to and including r. Isotropic anharmonicity of the potential field leads to a splitting of each r-term according to the orbital angular momenta l (l even when r is odd, and vice versa), as in Table I, column 4. Finally, spin-orbit coupling leads to the l-term splitting into $j=l\pm\frac{1}{2}$, columns 5 and 6, whose multiplicities are listed in column 7.

The "magic numbers" (column 8) follow at once on the assumption of a particularly marked splitting of the term with the highest angular momentum, resulting in a "closed shell structure" for each completed r-group, together with the highest j-term of the next succeeding r-group. This classification of states is in good agreement with the spins and magnetic moments of the nuclei with odd mass number, so far as they are known at present. The anharmonic oscillator model seems to us preferable to the potential well model,[2] since the range of the nuclear forces is not notably smaller than the nuclear radius.

A more detailed account will appear in three communications to Naturwissenschaften.[3]

TABLE I. Classification of nuclear states.

1 Oscillator-quantum number r	2 Multiplicity	3 Sum of all multiplicities	4 Orbital momentum l	5 Total angular momentum j	6 l_j-symbol	7 Multiplicities	8 Magic numbers
1	2	2	0	1/2	$s_{1/2}$	2	
2	6	8	1	3/2	$p_{3/2}$	4	
				1/2	$p_{1/2}$	2	
3			2	5/2	$d_{5/2}$	6	14
				3/2	$d_{3/2}$	4	
4	12	20	0	1/2	$s_{1/2}$	2	
			3	7/2	$f_{7/2}$	8	28
				5/2	$f_{5/2}$	6	
5	20	40	1	3/2	$p_{3/2}$	4	
				1/2	$p_{1/2}$	2	
			4	9/2	$g_{9/2}$	10	50
				7/2	$g_{7/2}$	8	
			2	5/2	$d_{5/2}$	6	
				3/2	$d_{3/2}$	4	
6	30	70	0	1/2	$s_{1/2}$	2	
			5	11/2	$h_{11/2}$	12	82
				9/2	$h_{9/2}$	10	
			3	7/2	$f_{7/2}$	8	
				5/2	$f_{5/2}$	6	
7	42	112	1	3/2	$p_{3/2}$	4	
				1/2	$p_{1/2}$	2	
			6	13/2	$i_{13/2}$	14	126
				11/2	$i_{11/2}$	12	
			4	9/2	$g_{9/2}$	10	

[1] See, e.g., H. A. Bethe and R. Bacher, Rev. Mod. Phys. 8, 82 (1937), pars. 32–34.
[2] Which anyhow does not lead to a very different term-sequence compared with that of an anharmonic oscillator, see reference 1.
[3] (a) Haxel, Jensen, and Suess, Naturwiss. (in press). (b) Suess, Haxel, and Jensen, Naturwiss. (in press). (c) Jensen, Suess, and Haxel, Naturwiss. (in press).

Shell structure of stable nuclei

Mayer and Jensen 1949

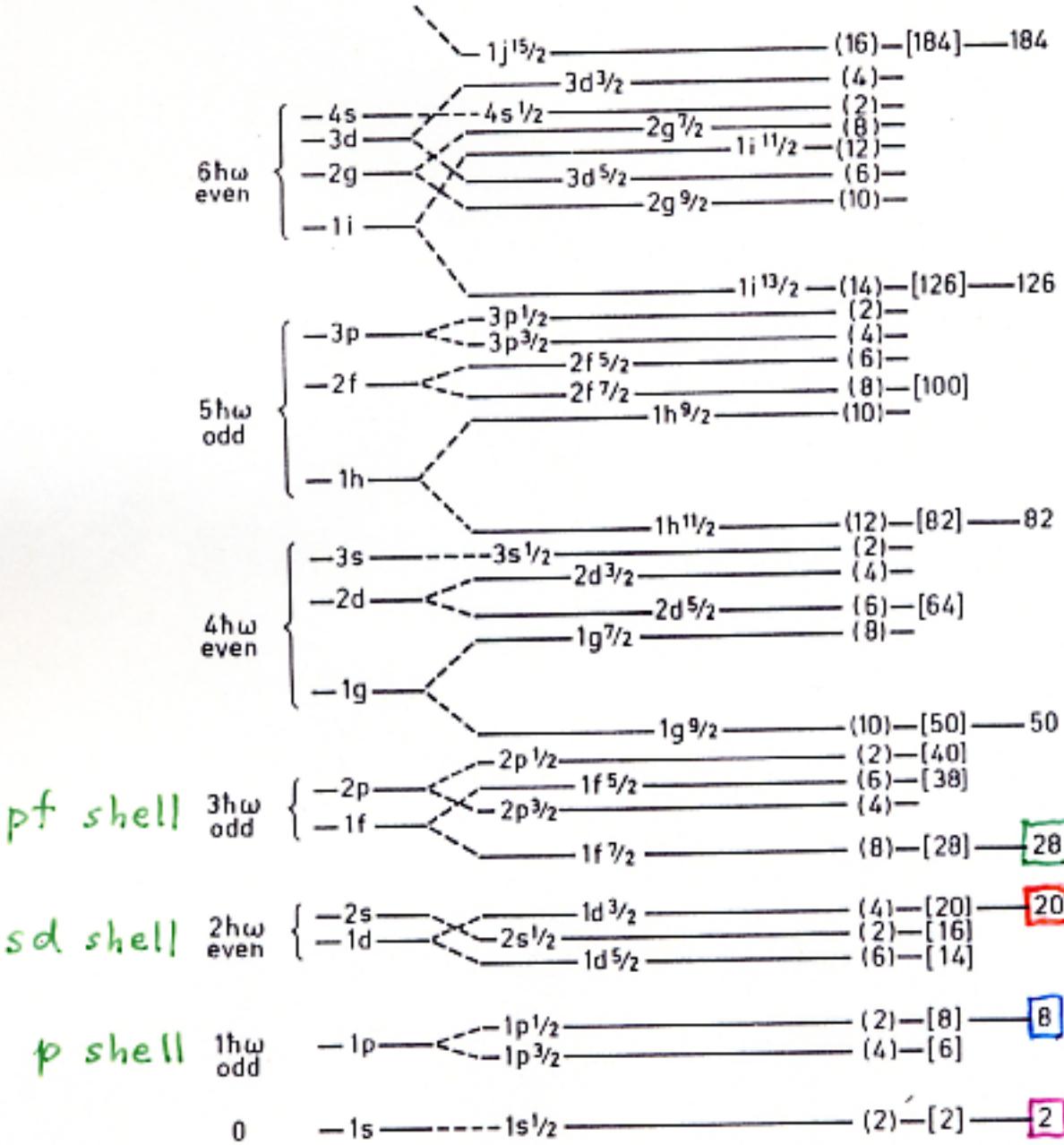

Figure 2-23 Sequence of one-particle orbits. The figure is taken from M. G. Mayer and J. H. D. Jensen, *Elementary Theory of Nuclear Shell Structure*, p. 58, Wiley, New York, 1955.

Harmonic Oscillator Potential + spin-orbit force

↑ magic number

↑ N=Z

Development of the Nuclear Shell Model -2

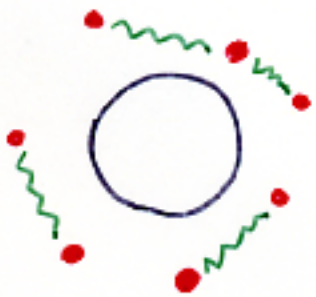

1970 ~

Calculations with many nucleons

p shell, sd shell, ^{208}Pb, ...

p shell : Cohen-Kurath

CK interaction

sd shell : Wildenthal-Brown

USD interaction

(~1980)

1990 ~ Present

"Large-scale" calculations

Conventional calc.

Monte Carlo calc.

"No-core" calc.

Barrett, Vary, Navratil, ...

Continuum Shell Model

Shell Model for Halo orbit

Shell model calculation in practice

Hamiltonian

$$H = \sum \varepsilon_i n_i + \sum_{\substack{i<j \\ k<l}} V_{ij,kl}\, a_i^\dagger a_j^\dagger a_l a_k$$

Single particle state

$$i : R_{n_i}(r) \underbrace{[Y_{l_i}(\theta,\varphi)}_{\text{orbital angular mom.}} u_i]^{(j_i)}_{m_i} v_i$$

n_i: node; u_i: spin ($\uparrow$ or $\downarrow$); v_i: isospin (p or n)

Slater determinant

$$\Psi_1 = a_{i_1}^\dagger a_{j_1}^\dagger \cdots a_{k_1}^\dagger |0\rangle$$

$$\Psi_2 = a_{i_2}^\dagger a_{j_2}^\dagger \cdots a_{k_2}^\dagger |0\rangle$$

$$\vdots$$

Hamiltonian matrix

$$H = \begin{bmatrix} * & * & * & * & \cdots \\ * & * & * & * & \cdots \\ * & * & * & \cdots & \\ \vdots & \cdots & & & \end{bmatrix}$$

$$H_{ij} \equiv \langle \Psi_i | H | \Psi_j \rangle$$

the number of Slater determinants

= dimension of the matrix

= Shell Model dimension

USD interaction

Brown & Wildenthal 1988

Table 3: USD parameters

Values of the two-body matrix elements and single-particle energies of the A = 18 version of the new empirical Hamiltonian for sd-shell model calculations. Units are MeV. The two-body matrix elements (2bme) $\langle (j_1,j_2)_{JT}|H^{2b}|(j_3,j_4)_{JT}\rangle$ are labeled by the indices of the j_i according to the convention of "1" for $0d_{5/2}$, "2" for $1s_{1/2}$ and "3" for $0d_{3/2}$ and by the values of twice the total angular momentum and total isospin of the two-body states, 2J and 2T. The two-body matrix elements for other values of A are obtained by multiplying these values by $(18/A)^{0.3}$. The values of the single-particle energies (spe) are independent of A.

sd shell USD

j_1	j_2	j_3	j_4	2J	2T	2bme
1	1	1	1	0	2	-2.8197
1	1	1	1	2	0	-1.6321
1	1	1	1	4	2	-1.0020
1	1	1	1	6	0	-1.5012
1	1	1	1	8	2	-0.1641
1	1	1	1	10	0	-4.2256
1	1	1	2	4	2	-0.8616
1	1	1	2	6	0	-1.2420
1	1	1	3	2	0	2.5435
1	1	1	3	4	2	-0.2828
1	1	1	3	6	0	2.2216
1	1	1	3	8	2	-1.2363
1	1	2	2	0	2	-1.3247
1	1	2	2	2	0	-1.1756
1	1	2	3	2	0	-1.1026
1	1	2	3	4	2	-0.6198
1	1	3	3	0	2	-3.1856
1	1	3	3	2	0	0.7221
1	1	3	3	4	2	-1.6221
1	1	3	3	6	0	1.8949
1	2	1	2	4	0	-1.4474
1	2	1	2	4	2	-0.8183
1	2	1	2	6	0	-3.8598
1	2	1	2	6	2	0.7626
1	2	1	3	4	0	-0.0968
1	2	1	3	4	2	-0.4770
1	2	1	3	6	0	1.2032
1	2	1	3	6	2	-0.6741
1	2	2	3	4	0	-2.0664
1	2	2	3	4	2	-1.9410
1	2	3	3	4	2	-0.4041
1	2	3	3	6	0	0.1887
1	3	1	3	2	0	-6.5058
1	3	1	3	2	2	1.0334
1	3	1	3	4	0	-3.8253
1	3	1	3	4	2	-0.3248
1	3	1	3	6	0	-0.5377
1	3	1	3	6	2	0.5894
1	3	1	3	8	0	-4.5062
1	3	1	3	8	2	-1.4497
1	3	2	2	2	0	2.1042
1	3	2	3	2	0	-1.7080
1	3	2	3	2	2	0.1874
1	3	2	3	4	0	0.2832
1	3	2	3	4	2	-0.5247
1	3	3	3	2	0	0.5647
1	3	3	3	4	2	-0.6149
1	3	3	3	7	0	2.0337
2	2	2	2	0	2	-2.1246
2	2	2	2	2	0	-3.2628
2	2	2	3	2	0	1.2501
2	2	3	3	0	2	-1.0835
2	2	3	3	2	0	0.0275
2	2	3	3	4	2	-4.2930
2	3	2	3	2	2	0.6066
2	3	2	3	4	0	-1.8194
2	3	2	3	4	2	-0.4064
2	3	3	3	2	0	0.3983
2	3	3	3	4	2	-0.5154
3	3	3	3	0	2	-2.1845
3	3	3	3	2	0	-1.4151
3	3	3	3	4	2	-0.0665
3	3	3	3	6	0	-2.8842

spe($0d_{5/2}$)	-3.94780
spe($1s_{1/2}$)	-3.16354
spe($0d_{3/2}$)	1.64658

• pairing (J=0, T=1)

▭ |V| > 3 MeV ○ T=0 $\langle j_1 j_2 J|V|j_1 j_2 J\rangle$

Shell model calculation in practice

Hamiltonian matrix

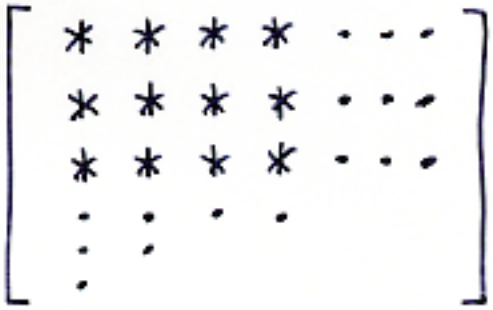

⇓ diagonalized *

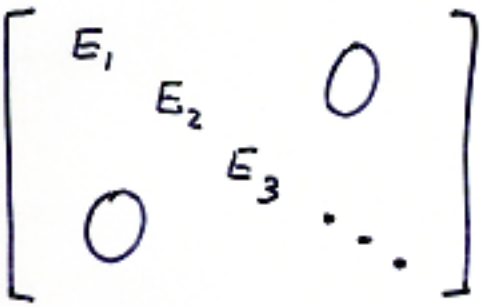

Eigenstate : $\Psi_i = \sum c_{ij} \Phi_j$

↑ Slater determinant

* Lanczos method

⇒ Lowest several eigenstates

Dimension

sd shell	up to 93710	^{28}Si
pf shell	up to 2×10^9	^{60}Zn
⋮	⋮	

Practical calculations

- Slater determinants Ψ_i $(i = 1, 2, \cdots)$
  - occupation numbers for each m state
    "m-scheme"
  - represented by bits on computer

- Example : $d_{5/2}$ 3 neutrons $M = \frac{1}{2}$

m	$5/2$	$3/2$	$1/2$	$-1/2$	$-3/2$	$-5/2$			
bit	□	□	□	□	□	□	□	□	···
Ψ_1	1	0	1	0	0	1	0	0	···
Ψ_2	0	1	1	0	1	0	0	0	···
Ψ_3	1	0	0	1	1	0	0	0	···

m-scheme dimension with $M = \frac{1}{2}$
$= 3$

Each Slater determinant
= a linear combination of
$J = \frac{9}{2}, \frac{5}{2}, \frac{3}{2}$

☐ Hamiltonian

$$H = \sum \varepsilon_i a_i^\dagger a_i + \sum \langle ij|V|kl\rangle a_i^\dagger a_j^\dagger a_l a_k$$

Example (of the previous page)

m	$5/2$	$3/2$	$1/2$	$-1/2$	$-3/2$	$-5/2$
Ψ_1	1	0	1	0	0	1
Ψ_3	1	0	0	1	1	0

$\Uparrow$

$\langle 1/2, -5/2 | V | -1/2, -3/2 \rangle$

Hamiltonian Matrix

$$H = \begin{bmatrix} \langle \Psi_1|H|\Psi_1\rangle & \langle \Psi_1|H|\Psi_2\rangle & \langle \Psi_1|H|\Psi_3\rangle \\ \langle \Psi_2|H|\Psi_1\rangle & \cdot & \cdot \\ \langle \Psi_3|H|\Psi_1\rangle & \cdot & \cdot \end{bmatrix}$$

$\Downarrow$ diagonalization

$$H = \begin{bmatrix} \varepsilon_1 & & 0 \\ & \varepsilon_2 & \\ 0 & & \varepsilon_3 \end{bmatrix}$$

Eigenstate : $\sum x_i \Psi_i$

↳ Also eigenstate of $\vec{J}\cdot\vec{J}$

($J = \frac{9}{2}, \frac{5}{2}$, or $\frac{3}{2}$)

Basics of shell model calculations

Valence nucleons : explicitly treated

Nucleons in the closed and in higher shells :

Effects are included through renormalizations of particle-hole excitations (surface vibrations)

Effective interactions (pairing, quadrupole, etc.)

Effective charges

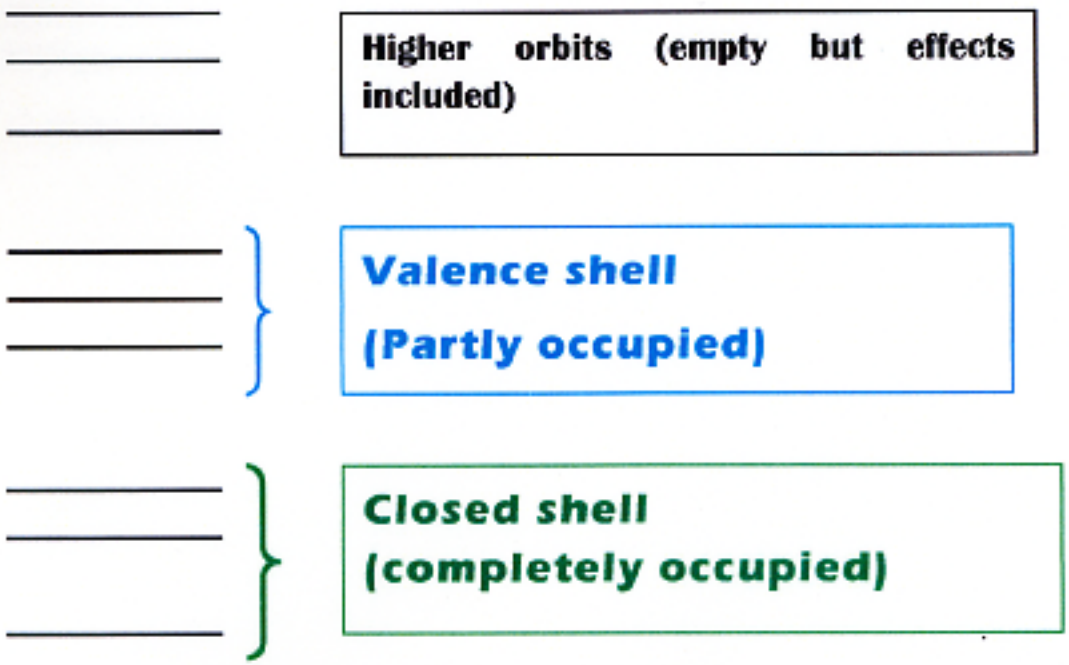

Truncation of Shell Model Space

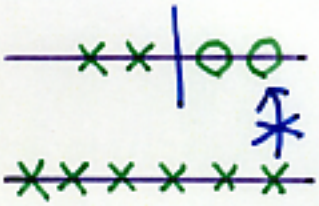

truncation

⇓

maximum (or minimum)

number of nucleons

is set for certain orbits

⇓

decrease of dimension

more feasible

less accurate

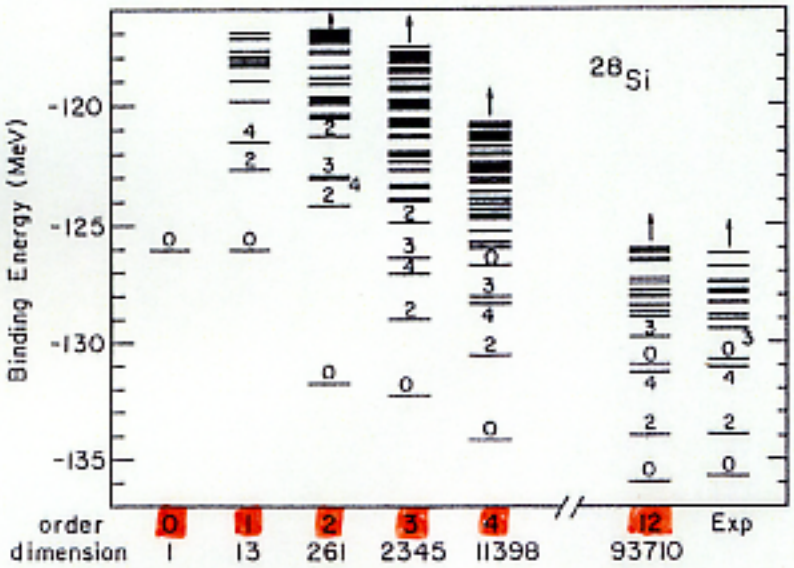

Figure 1 Binding energies of levels in ^{28}Si as a function of the number of excitations from the $d_{5/2}$ orbital (see Section 2).

example above: the number of nucleons* in $2s_{1/2} + 1d_{3/2}$ of ^{28}Si is changed from 0 to 12. (left) (right)

Computer Programs for conventional shell-model calculations

OXBASH : Oxford - Buenos-Aires Shell Model

~ 100×10^3 dim.

$(SM)^2$: Strasbourg - Madrid

ANTOINE Shell Model

~ several million dim.

↳ 20 ~ 100

VECSSE : Vectorized Shell Model code by Sebe et al.

~ 2 million (or more) dim.

↳ 20 ~ 100

⋮

MSHELL ~ 100 million dim

The Lanczos method is used for diagonalization of large matrix.

Developments of Shell Model calculations vs. Evolution of Computers

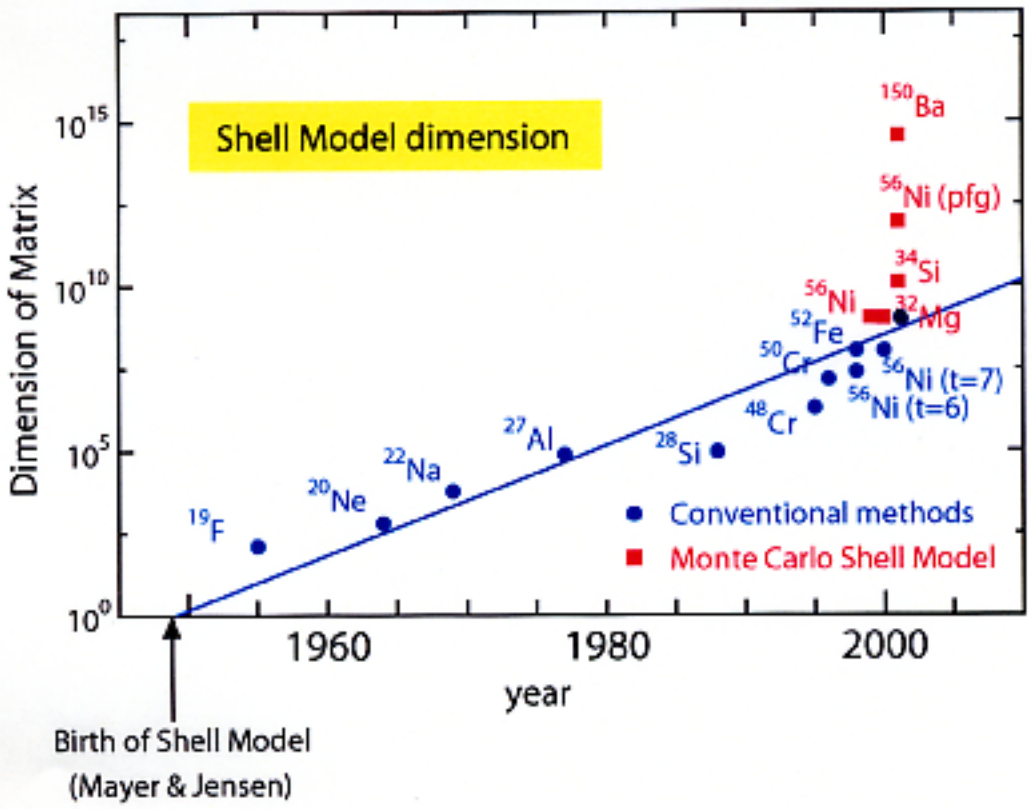

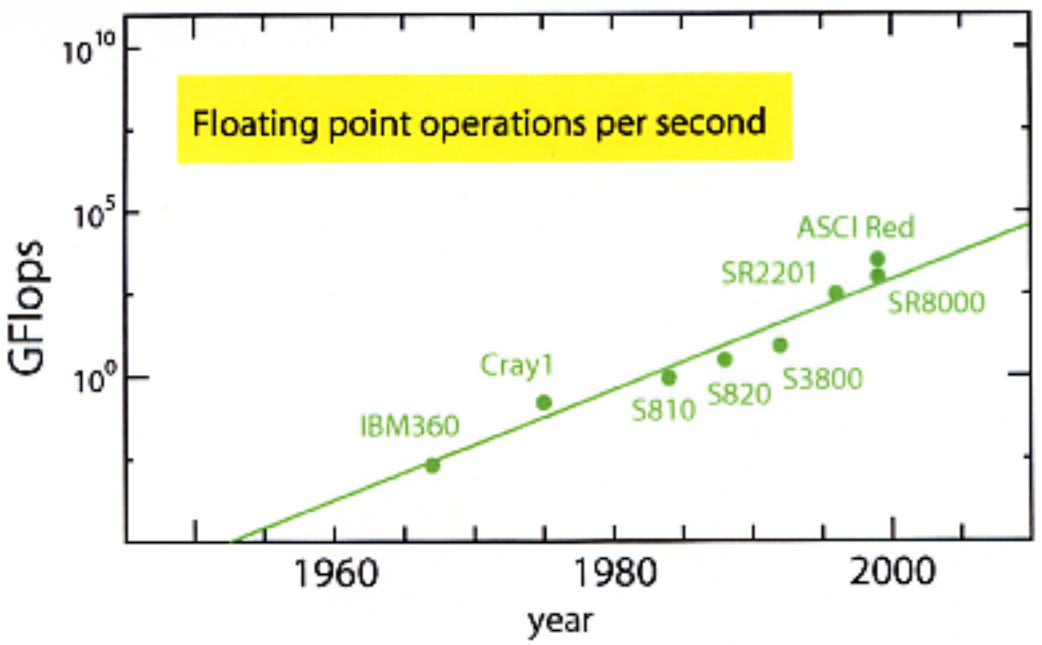

Lines of both figures indicate a growth of 10^{5}/30 years

The conventional shell-model calculation with a full major shell has been successful up to A~50, but it is not feasible for heavier nuclei due to enormously large dimensions.

⇒ **Stochastic approaches**

[1] **Shell Model Monte Carlo (SMMC)**

1992~
Auxiliary Field Monte Carlo calculations
S.E. Koonin et al., Phys. Report 278, 1 (1997)

Ground-state properties
Minus-sign problem → various restrictions

[2] **Quantum Monte Carlo Diagonalization (QMCD)**

1995~
with M. Honma and T. Mizusaki

PRL 75, 1284 (95)
⋮
PRL 81, 1588 (98)

Application to Nuclear Shell Model
⇨ Monte Carlo Shell Model

Imaginary Time Evolution

For a state $|\Psi^{(0)}\rangle = \sum_i c_i |\Psi_i\rangle$,

($|\Psi_i\rangle$: eigenstate of H)

$$e^{-\beta H} |\Psi^{(0)}\rangle = \sum_i e^{-\beta E_i} \cdot c_i |\Psi_i\rangle$$

$$\longrightarrow e^{-\beta E_1} \cdot c_1 |\Psi_1\rangle$$

$\beta \to$ large ; $|\Psi_1\rangle$: ground state

Suppose the Hamiltonian takes a simple form

$$\boxed{H = \frac{1}{2} V_\alpha O_\alpha^2} \quad (V_\alpha < 0)$$

O_α : one-body operator

Hubbard-Stratonovich (HS) transformation

$$e^{-\beta H} = e^{-\beta \frac{1}{2} V_\alpha \boxed{O_\alpha^2}}$$

$$= \int_{-\infty}^{\infty} \boxed{d\sigma_\alpha} \sqrt{\frac{\beta |V_\alpha|}{2\pi}} \underbrace{e^{-\frac{\beta}{2}|V_\alpha| \boxed{\sigma_\alpha^2}}}_{\text{Gaussian}} \cdot e^{-\beta V_\alpha \boxed{\sigma_\alpha} \boxed{O_\alpha}}$$

$$\Rightarrow \sum \quad e^{-\beta V_\alpha \sigma_\alpha O_\alpha}$$

MC : σ_α

↳ Monte Carlo sampling with a Gaussian weight

Hubbard – Stratonovich (HS) transformation

HS transformation

We start with $\int_{-\infty}^{\infty} dx\, e^{-ax^2} = \sqrt{\frac{\pi}{a}} \qquad (a>0)$

$$\int_{-\infty}^{\infty} dx\, e^{-a(x+c)^2} = \sqrt{\frac{\pi}{a}}$$

$$= \int_{-\infty}^{\infty} dx\, e^{-a(x^2+2xc+c^2)} = e^{-a c^2} \times \int_{-\infty}^{\infty} dx\, e^{-ax^2-2axc}$$

$$e^{a c^2} = \sqrt{\frac{a}{\pi}} \int_{-\infty}^{\infty} dx\, e^{-a x^2 - 2a x c} \quad \cdots\cdots\cdots (*)$$

Now, we consider the imaginary time evolution operator:

$$e^{-\beta H} = e^{\cdots - \beta \frac{1}{2} V_\alpha O_\alpha^2 - \cdots}$$

$$H = \tfrac{1}{2} V_\alpha O_\alpha^2$$

If $V_\alpha < 0$,

$$-\beta \tfrac{1}{2} V_\alpha \to a, \qquad O_\alpha \to c$$

$$\hookrightarrow \beta \cdot \tfrac{1}{2} \cdot |V_\alpha|$$

Also x is written as σ_α

$$e^{-\beta \frac{1}{2} V_\alpha O_\alpha^2} = \int_{-\infty}^{\infty} d\sigma_\alpha \sqrt{\frac{\beta(-V_\alpha)}{2\pi}}\; e^{-\frac{\beta}{2}(V_\alpha \sigma_\alpha^2 + 2 V_\alpha \sigma_\alpha O_\alpha)} \quad \cdots\cdots\cdots (*)$$

$$= \int_{-\infty}^{\infty} d\sigma_\alpha \sqrt{\frac{\beta(-V_\alpha)}{2\pi}}\; G(\sigma_\alpha)\; e^{-\beta |V_\alpha| \sigma_\alpha O_\alpha}$$

$$G(\sigma_\alpha) = e^{-\frac{\beta}{2}|V_\alpha|\sigma_\alpha^2}$$

integration over σ_α

(auxiliary field)

Introducing a one-body hamiltonian,

$$h(\sigma_\alpha) \equiv v_\alpha \sigma_\alpha O_\alpha ,$$

the ground state can be written as

$$|\Phi_g\rangle \sim \sum_{MC:\sigma_\alpha} e^{-\beta h(\sigma_\alpha)} |\Phi^{(0)}\rangle$$

with Gaussian weight

Thus,

$$E_g \sim \frac{\langle \Phi^{(0)} | H \sum_{MC} e^{-\beta h(\sigma_\alpha)} |\Phi^{(0)}\rangle}{\langle \Phi^{(0)} | \sum_{MC} e^{-\beta h(\sigma_\alpha)} |\Phi^{(0)}\rangle}$$

The sampling is carried out by the Metropolis method.

⇩

Shell Model Monte Carlo (SMMC)

Koonin, Johnson, Ormand, Dean, Langanke, ... Alhassid, ...
cf. Phys. Rep. 278 (1997) 1

- ground-state properties
  energy, sum rules
  response functions (→ info. on excited states)
- (minus) sign prolbem
  most of realistic int. → difficulty

Introducing a one-body hamiltonian,

$$h(\sigma_\alpha) \equiv V_\alpha \sigma_\alpha O_\alpha ,$$

the ground state can be written as

$$|\Psi_g\rangle \sim \sum_{MC:\sigma_\alpha} e^{-\beta h(\sigma_\alpha)} |\Psi^{(0)}\rangle$$

$(\beta \to \text{large})$

This process produces all basis vectors needed for $|\Psi_g\rangle$

We then define

$$\Psi(\sigma_\alpha) \equiv e^{-\beta h(\sigma_\alpha)} |\Psi^{(0)}\rangle$$

as a basis vector.

We diagonalize the Hamiltonian in a subspace spanned by a small number of $\Psi(\sigma_\alpha)$'s.

⇨ Quantum Monte Carlo Diagonalization

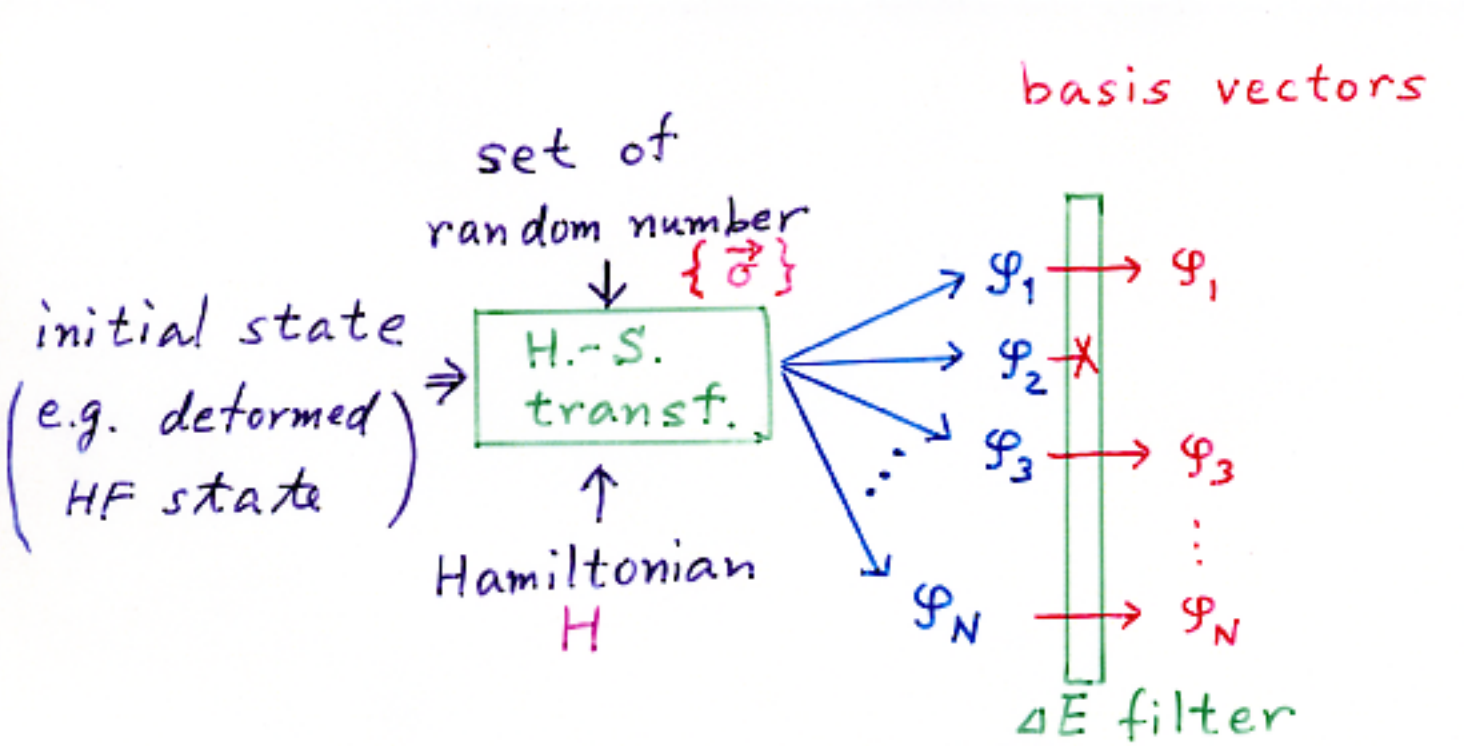

$$|\varphi_i\rangle \propto \prod_{k=1}^{N_t} e^{-\Delta\beta\, h(\vec{\sigma}_k)} |\varphi_0\rangle$$

$|\varphi_0\rangle$: initial state.

$$h(\vec{\sigma}) = \sum_\alpha (E_\alpha + s_\alpha V_\alpha \sigma_\alpha) O_\alpha$$

σ_α: random numbers

$s_\alpha = \begin{cases} 1 & V_\alpha < 0 \\ i & V_\alpha > 0 \end{cases}$

for the Hamiltonian

$$H = \sum_\alpha E_\alpha O_\alpha + \frac{1}{2} \sum V_\alpha O_\alpha^2$$

E_α: s.p.e. $\quad$ V_α: two-body int.

O_α : one-body operator

We diagonalize H in a subspace

$\{ \varphi_0, \varphi_1, \cancel{\varphi_2}, \cdots, \varphi_N \}$.

ΔE filter → selection (ground or excited)

$\Rightarrow$ energy eigenvalue,
wave functions,
transition matrix elements

Quantum Monte Carlo Diagonalization method

(QMCD)

Methodological development

Basic (and naïve) formulation

$$\Phi(\sigma) = e^{-\beta h(\sigma)} \Phi_0 \qquad \sigma : \text{a set of random numbers}$$

Slater det. **Slater det.**

Honma *et al.*, Phys. Rev. Lett. **75**, 1284 (1995)

Major Improvements

(1) Mean Field (e.g., Hartree-Fock) is utilized

Φ_0 : Hartree-Fock ground (or local-minimum) state

$h(\sigma) = h_{MF}$ + fluctuation part by σ

Mean Field (independent of σ)

(2) Stochastic noise is reduced in the basis

Refinement of each basis ($\sigma \rightarrow \sigma + \Delta\sigma$)

$\Rightarrow$ <u>fewer</u> bases for the same precision

Compression of the Hilbert subspace in which the shell-model Hamiltonian is diagonalized

(3) Full restoration of symmetries

Isolated quantal system $\Rightarrow$ symmetries (angular momentum, parity, *etc.*)

Symmetry restored matrix elements of the Hamiltonian by the projection method.

Mizusaki *et al.*, Phys. Rev. C **53**, 2786 (1996)

Honma *et al.*, Phys. Rev. Lett. **77**, 3315 (1996)

Otsuka *et al.*, Phys. Rev. Lett. **81**, 1588 (1998)

4.4 Path Integral interpretation of QMCD basis generation

The basis generation in eq. (29) can be interpreted in terms of the path integral. Equation (29) indicates that the state evolves in the imaginary time with one-body fields O_α in eq. (23). The interval of this imaginary time evolution is given by $\Delta\beta$, and the strength of one-body fields are determined by a vector of random numbers, $\vec{\sigma}$. In other words, at each "time", the path of evolution is given by the vector $\vec{\sigma}$, and a set of $\vec{\sigma}$'s finally determine the QMCD basis after N_t steps. Thus, one can interpret the QMCD basis generation from the viewpoint of the path integral: the path leads us to the basis.

4.5 Slater determinant basis

In practical shell model calculations, it is convenient to adopt basis vectors in the form of Slater determinants:

$$|\Phi\rangle = \prod_{\alpha=1}^{N} a_\alpha^\dagger |-\rangle, \tag{30}$$

where N denotes the number of valence nucleons, $|-\rangle$ is an inert spherical core, and $a_\alpha^\dagger$ represents the nucleon creation operator in a single-particle state α.

First, this single-particle state α is a canonical one and is a linear combination of the spherical single-particle states,

$a_\alpha^\dagger$ canonical (or deformed)

$$a_\alpha^\dagger = \sum_{i=1}^{N_{sp}} c_i^\dagger D_{i\alpha}, \tag{31}$$

$c_i^\dagger$ { creation op. of spherical single-particle state

where the state i means a usual spherical single-particle state, $c_i^\dagger$ is its creation operator, and D's are amplitudes. We can specify the basis vector $|\Phi\rangle$ in terms of an $N_{sp} \times N$ complex matrix D.

We now show how the state in eq. (30) is transformed by the process in eq. (29). We introduce an operator,

$$X \equiv \sum_{ij} t_{ij} c_i^\dagger c_j, \tag{32}$$

where t_{ij} denotes a complex number. The basic step of the operation in eq. (29) can be represented schematically by,

form of basis generation

$$e^X |\Phi\rangle = \prod_{\alpha=1}^{N} e^X a_\alpha^\dagger e^{-X} |\tilde{\Phi}\rangle. \qquad X = -\beta h(\vec{\sigma}) \tag{33}$$

The action,

$$e^X a_\alpha^\dagger e^{-X}, \tag{34}$$

means the replacement of the D matrix in eq. (31) with a new matrix,

$$D' = e^T D, \qquad T = [t_{ij}] \tag{35}$$

where T denotes the matrix $[t_{ij}]$ and e^T means the exponential of the matrix T. Thus, the basis generation in eq. (29) implies the transformation of the matrix D as in eq. (35) with an appropriate matrix T.

We emphasize that the form of a Slater determinant remains in this process. Namely, throughout the basis-search process presented in subsect. 4.3, a more important basis vector is looked for within a single Slater determinant.

4.6 Major methodological improvements

The procedure presented so far is the first version of QMCD. Although it works well for simple systems [6], it turned out that, in order to carry out realistic large-scale shell-model calculations, we have to improve the method as discussed in the following.

4.6.1 Basis generation around the mean field solution

Since the number of manageable basis vectors is finite in practice, we should select basis vectors of higher importance. We thus choose $|\Psi^{(0)}\rangle$ from a Hartree-Fock (HF) local minima or some states of similar nature, although $|\Psi^{(0)}\rangle$ is not specified in eq.(29). Note that the present HF calculation means the one with the shell-model Hamiltonian in the given single-particle space. We emphasize that the Hartree-Fock ground state is the "best" single Slater determinant by definition, and fits well into the present picture.

First, we rewrite the Hamiltonian in eq. (22) by introducing c-numbers, denoted by c_α, as,

$$H = \sum_{\alpha=1}^{N_f} [E_\alpha O_\alpha + \frac{1}{2} V_\alpha (O_\alpha - c_\alpha)^2 + V_\alpha O_\alpha c_\alpha - \frac{1}{2} V_\alpha c_\alpha^2]. \quad (36)$$

c-number

The one-body Hamiltonian $h(\vec{\sigma}_n)$ in eq.(23) is then given as

$$h(\vec{\sigma}_n) = \sum_\alpha [(E_\alpha + V_\alpha c_\alpha) O_\alpha + s_\alpha V_\alpha \sigma_{\alpha n} O_\alpha], \quad (37)$$

where the c-number $-\sum_\alpha s_\alpha V_\alpha \sigma_{\alpha n} c_\alpha$ is dropped off since it does not change the wave functions, apart from the normalization and phase in eq. (29). In this expression, the first one-body term $\sum_\alpha (E_\alpha + V_\alpha c_\alpha) O_\alpha$ on the right-hand side includes effects coming from the two-body interaction. The values of c_α's can be taken as we like, and are set so that this first one-body term becomes the single-particle mean field of the HF or other similar calculations. We thus define,

$$h_{\rm MF} = \sum_\alpha (E_\alpha + V_\alpha c_\alpha) O_\alpha. \quad (38)$$

adjusted so that $h_{\rm MF}$ is obtained

With this $h_{\rm MF}$, the one-body Hamiltonian used in eq. (29) becomes,

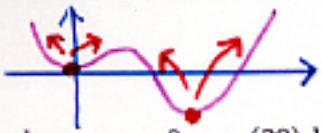

$$h(\vec{\sigma}_n) = h_{\rm MF} + \sum_\alpha V_\alpha s_\alpha \sigma_\alpha O_\alpha. \quad (39)$$

If we keep $\sigma_\alpha = 0$, eq. (29) becomes simply the projection onto the mean-field solution corresponding to the $h_{\rm MF}$. Since $h_{\rm MF}$ is independent of the auxiliary fields σ_α and the sampling is made around $\sigma_\alpha = 0$, the QMCD bases $|\Phi(\sigma)\rangle$'s are generated around a local minimum designated by the relevant mean field.

This process is extremely useful for yrast states by combining with the angular momentum projection techniques discussed later. If a state in a pronounced local minimum is studied, $h_{\rm MF}$ can be set there. On the other hand, this process may not be very relevant to non-yrast states without such structure.

4.6.2 Restoration of angular momentum and parity

The nucleus is an isolated system and conserves several symmetries, including the rotational symmetry and the parity symmetry. In the QMCD generation of the basis vectors, those symmetries should be restored as more basis vectors are added, because eigenstates have those symmetries. On the other side, in order to restore the symmetries, we need generally a superposition of a number of basis vectors mutually correlated in a specific way. For instance, the parity can be restored by having a proper superposition of two wave functions connected by the parity operation. However, if one wants to fulfill this superposition by basis generation driven by random numbers, it should become a very slow process: for instance, it is nearly impossible to hit right on the other partner wave function required in this parity superposition.

On the other hand, the parity and angular momentum are geometrical symmetries conserved exactly. Moreover, those symmetries give quantum numbers to which calculated physical quantities are very sensitive. We therefore introduce methods for external and exact restoration of those symmetries. The parity is conserved simply by the parity projection which is not difficult and can be done by the superposition of a wave function and its parity-reversed partner. We include this for each step of the basis generation, if necessary.

◇ Compression of QMCD space

Stochastic basis generation is not efficient because of "noise".

$$\Psi \sim a_1 \xi_1 + a_2 \xi_2 + \cdots\cdots + a_N \xi_N$$

$n \ll N$ compressed

$$\sim c_1 \varphi_1 + \cdots + c_n \varphi_n$$

The compression of Hilbert space used for the diagonalization is carried out by searching more favorable basis, φ_i.

◇ Symmetry restoration

An isolated many-body system, e.g. a nucleus, has symmetries: angular momentum, parity, ···

$$\Phi(\vec{\sigma}) = e^{-\beta h(\vec{\sigma})} |\Phi^{(0)}\rangle$$

$\Phi(\vec{\sigma})$: no symmetry

$h(\vec{\sigma})$: no symmetry conservation

Stochastic restoration is practically impossible. (in eigenstate (Ψ))

⇨ Each basis is projected.

Symmetry restoration

An isolated many-body system, e.g., a nucleus, has symmetries: angular momentum, parity, etc.

$$\Phi(\sigma) = \prod_{i=1}^{N_t} e^{-\Delta\beta \cdot h(\vec{\sigma}_i)} \, |\Phi^{(0)}\rangle$$

- $\Phi(\sigma)$ → no symmetry
- $e^{-\Delta\beta \cdot h(\vec{\sigma}_i)}$ → no symmetry conservation
- $|\Phi^{(0)}\rangle$ → symmetry can be violated (deformed H.F.)

Stochastic restoration of the symmetries in the eigenstate Ψ is practically impossible.

⇩

Projection

$$\langle \Phi(\sigma_i) | H P | \Phi(\sigma_j) \rangle$$

P ↑ projection operator

numerical calculations

parallel computing

Full projection of angular momentum

QMCD basis

$$|\Phi(\sigma)\rangle \propto \prod e^{-\Delta\beta \cdot h(\vec{\sigma})} |\Phi^{(0)}\rangle$$

↓ deformed

$h(\vec{\sigma})$: not a scalar in general

$|\Phi^{(0)}\rangle$: deformed HF local minimum

Projection

$$|\Phi(\sigma)\rangle \longrightarrow P_{J,M} |\Phi(\sigma)\rangle$$

- Actual projection is carried out only when <u>matrix elements</u> are calculated
- Projection = rotation with Euler angles
  - ↳ discretized at <u>mesh points</u>

$$\langle \Phi(\sigma_i) | H P_{J,M} | \Phi(\sigma_j) \rangle$$

$$\propto \int d\alpha d\beta d\gamma \sin\beta \; \Phi(\sigma_i)^* H D^{J}_{MK}(\gamma,\beta,\alpha) e^{i\gamma J_z} e^{i\beta J_y} e^{i\alpha J_z} \Phi(\sigma_j)$$

- $\int d\alpha d\beta d\gamma \sin\beta$: summation over mesh points
- $e^{i\gamma J_z} e^{i\beta J_y} e^{i\alpha J_z}$: unitary transf.

* Distribution over K is optimized.

Remarks on the QMCD method

The bases used for diagonalization of the Hamiltonian are generated by

$$\Phi(\sigma) = e^{-\beta h(\sigma)} \Phi_0 \qquad \sigma : \text{a set of } \textbf{random numbers}$$

Slater det. Slater det.

so that larger gain of the energy eigenvalue is obtained. Only "good" $\Phi(\sigma)$'s are kept.

⇒ QMCD is a stochastic truncation scheme of bases according to contributions to the total energy.

- Mean field solutions are included as natural first choices
  Hartree-Fock ground state = best single Slater determinant
- Contrast to the ***conventional*** shell model calculations with truncations in terms of single-particle configurations, *etc.*

The QMCD method can be characterized as the ***Importance Truncation*** scheme.

Application of the QMCD method to the Nuclear Shell Model

⇒ ***Monte Carlo Shell Model***

- *No minus-sign problem in the QMCD method.*

- The QMCD method can be used for many-body systems in general.

Test of QMCD calculation (phase III)

$^{48}Cr = {}^{40}Ca + \underbrace{4n + 4p}_{pf\ shell}$

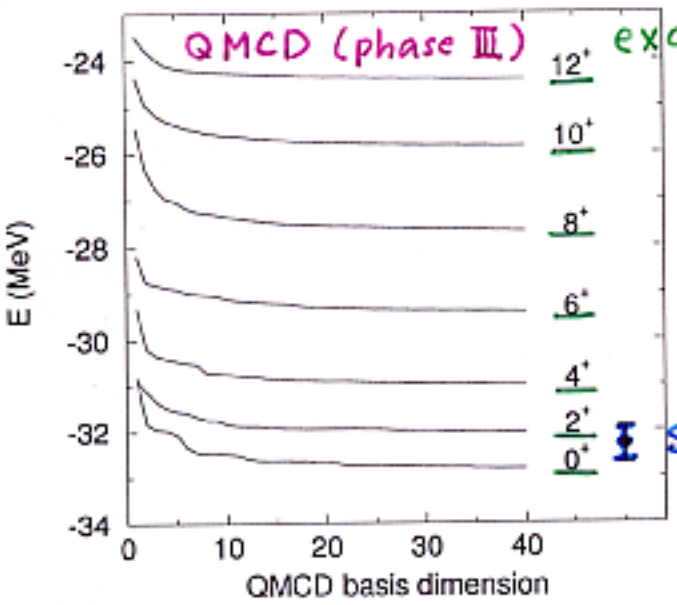

exact : Caurier et al. P.R. C50, 225 (1994)

~ 2 million dimension

SMMC : Langanke et al. P.R. C52, (95) 718

$E_g = -32.3 \pm 0.4$ (MeV)

(T = 0.5 MeV)

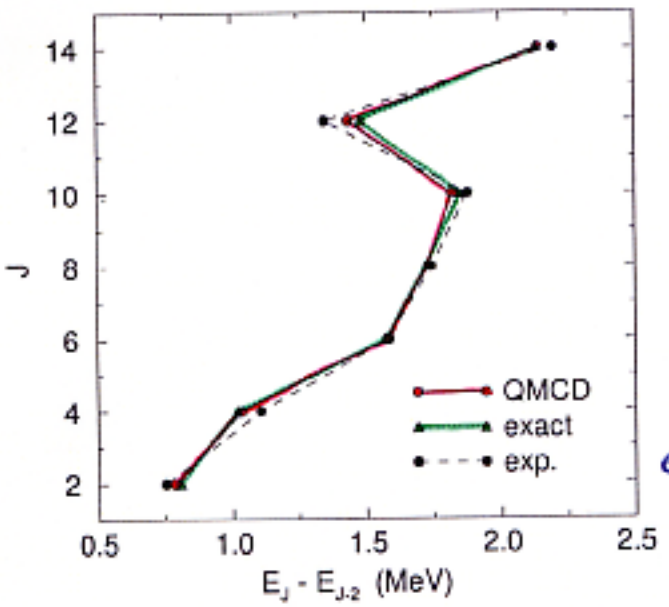

exp : Lenzi et al. Z. Phys. A354 (96) 117

$E_J - E_{J-2}$ (MeV)

The KB3 interaction is commonly used in the calculations.

See T.O. et al, J. Phys. G. 25 (1999) 699

Comparison between conventional and Monte-Carlo shell-model calculations

- Conventional method

all components (Slater determinants)

$H =$  diagonal-ize 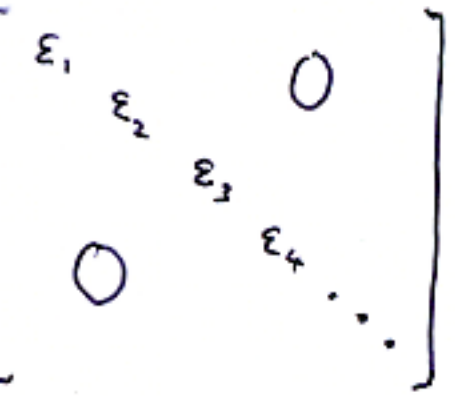

dimension 10^4 (^{24}Mg)

$\sim 10^9$ (^{32}Mg) $\sim \cdots$

- MCSM : importance truncation

$\psi \rightarrow e^{-\beta h(\sigma)} \psi$

Slater det. Slater det.

$H =$ 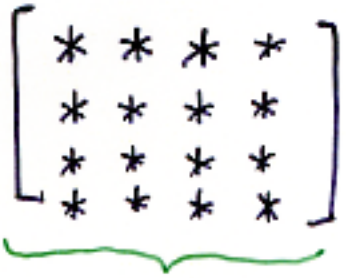 diagonalize 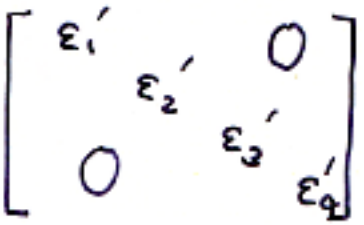

selected components

$\varepsilon_i' \approx \varepsilon_i$

dimension 30~50 / eigenstate

Practical Performance

for a typical problem with original dimension of $\sim 10^9$.

Parallel machine with 30 CPU's

1 CPU = Alpha 21264 (500 MHz)

- ground state

  QMCD dimension ~ 20

  $\sim$ 1 day

- yrast + yrare state

  QMCD dimension $\sim 20 + 40$

  $\sim$ 8 days

  - # of mesh points in the angular momentum projection

    $\sim 20000 \sim 25^3$

  - To get one good basis state, discard ~ 300 candidates.

    30 QMCD dim. $\Rightarrow$ 10 000 candidates discarded

Features of the Monte Carlo Shell Model

(1) Many orbits can be treated as being active (*i.e.*, valence).

Because of this large space, a wide variety of states in the same nucleus can be obtained from a common Hamiltonian.

⇒ ***Feasibility along the energy axis***

Example: spherical, deformed and superdeformed states in ^{56}Ni

(2) Many particles can be treated as being active (*i.e.*, valence).

Because of this feasibility, a wide range of nuclei can be described within the same framework.

⇒ ***Feasibility along the particle-number (or isospin) axis***

Example: Spherical-deformed phase transition in heavy nuclei

The same features are even more crucial in studying and predicting the structure of **exotic nuclei with extreme isospin.**

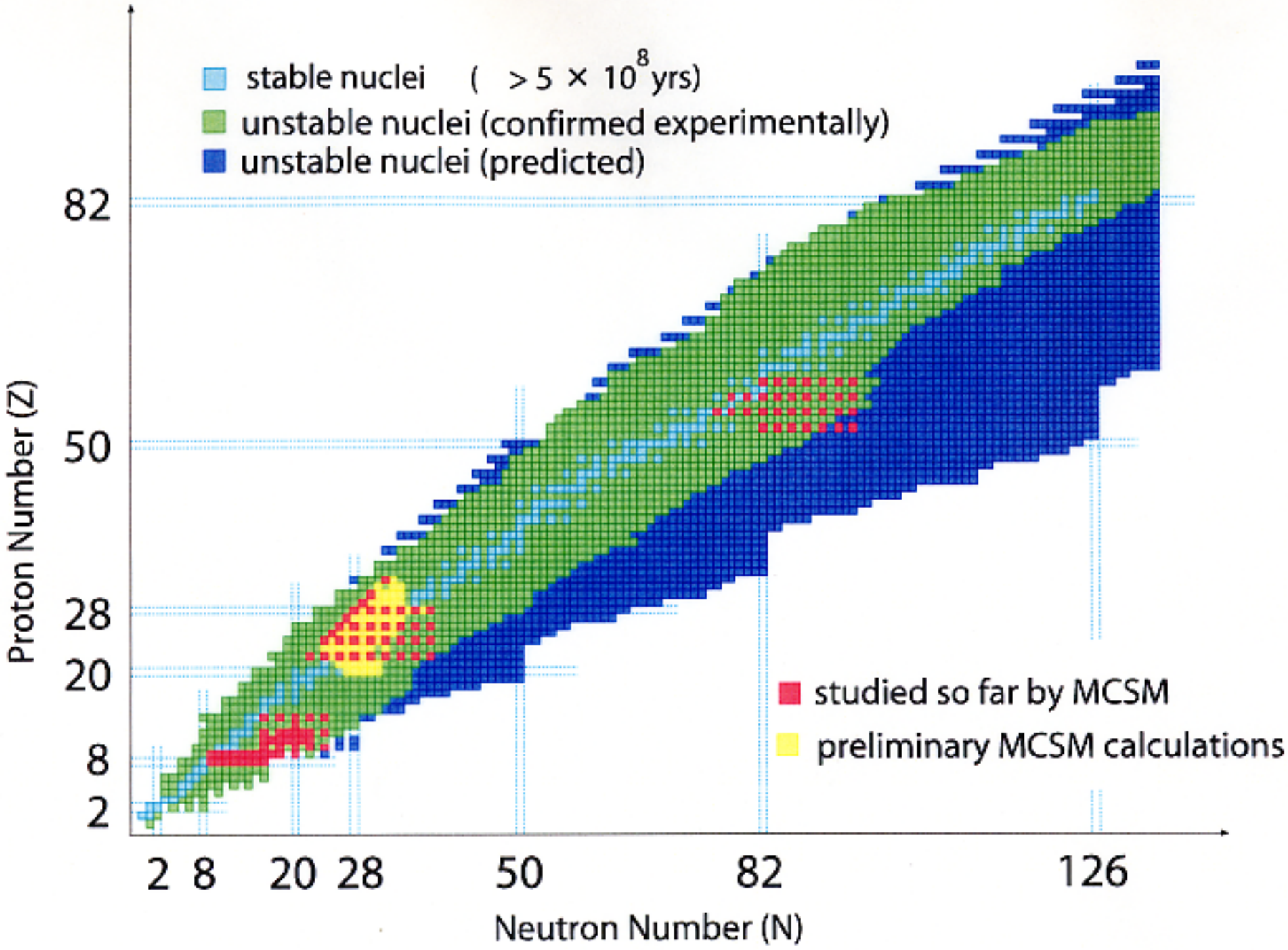
stable nuclei (> 5 × 10^8 yrs)
unstable nuclei (confirmed experimentally)
unstable nuclei (predicted)
studied so far by MCSM
preliminary MCSM calculations
Proton Number (Z)
Neutron Number (N)
2
8
20
28
50
82
126

$B(E2; 0^+ \to 2^+)$ values

Radford et al.

PRL 88, 222501 (2002)

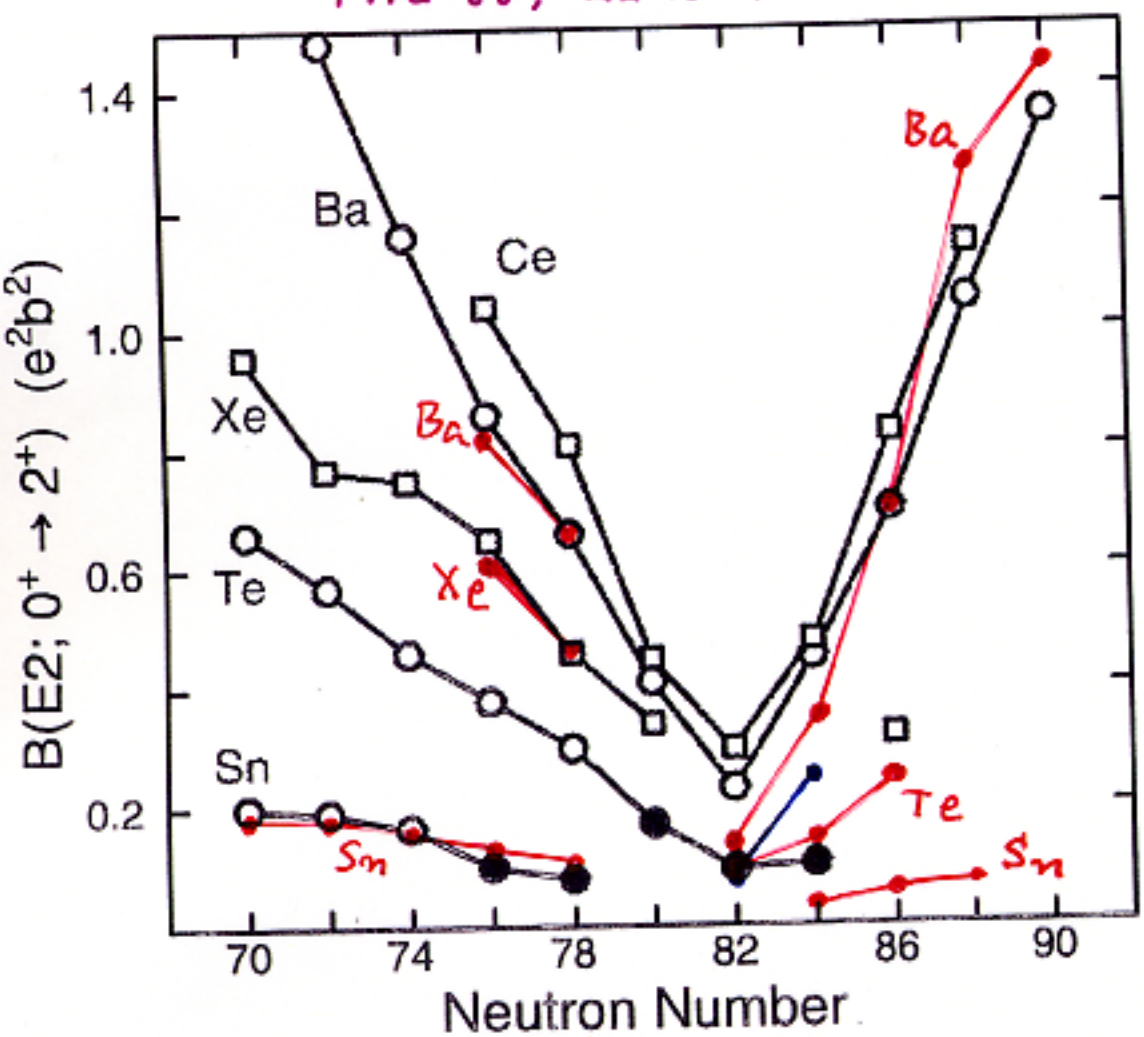

FIG. 2. Values of $B(E2;0^+ \to 2_1^+)$ for even-even Sn, Te, Xe, Ba, and Ce isotopes around neutron number $N = 82$. Open symbols are adopted values from Ref. [8], while filled symbols are from the present work (Te) and from Refs. [4,10] (Sn).

present calc. (Shimizu et al. MCSM)

Covello et al. for Te

Summary

MCSM (Monte Carlo Shell Model)

20~50 bases with projection onto J and M

against the dimension of the original Hilbert space : 10^4 ~ 10^9 ~ 10^{14} ~

^{24}Mg ^{32}Mg rare earth

^{56}Ni

diagonalization of Hamiltonian ⇒

levels, wave functions,

transition matrix elements

MCSM : *Importance truncation* scheme to the full calculation

- many valence orbits

  more than one major shell

- many valence particles

  so far up to 26

- natural relation to mean field theories (HF, GCM, HFB, *etc.*)

- no minus sign problem

Nuclear Theory Activities in Japan for RIBF

[1] Computational nuclear physics with massive parallel computer for studies of unstable nuclei

A massive parallel computer, "Alphleet", dedicated to large-scale nuclear structure calculations

140 most advanced Alpha CPU's (called ev6 or 21264)

Alphleet (Alpha Fleet) computer (RIKEN, April 1999)

Monte Carlo Shell Model calculations

Neutron-rich O-Ne-Mg isotopes

Dripline, mass, level scheme, deformation

Multi Gaussian Basis calculations for light nuclei

^{11}Li : Neutron halo

2nd generation of Alphleet parallel system

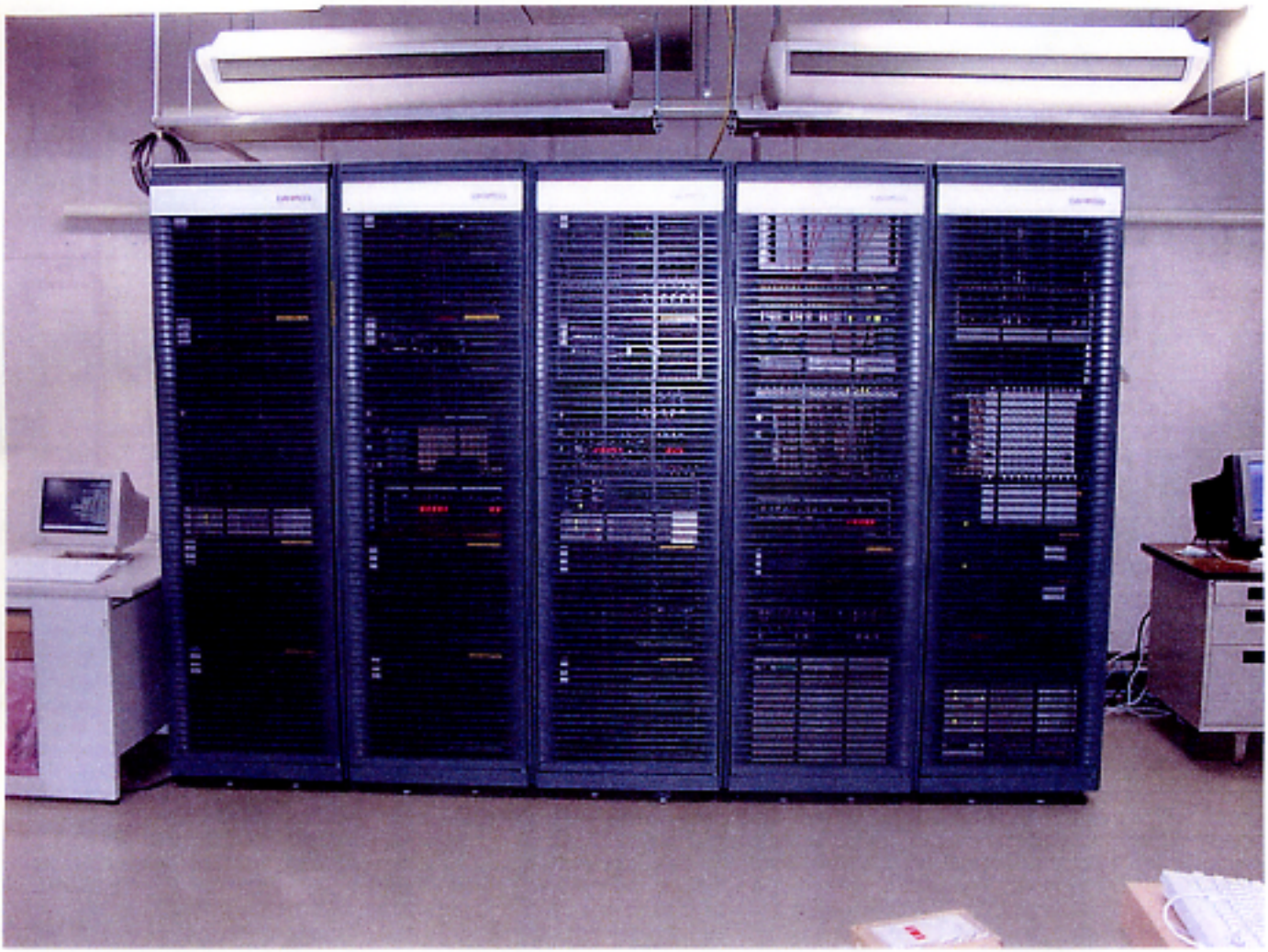

- 科学研究費 特別推進研究 (代表者 大塚)
  平成 13 ~ 17 年度
- 理研 - CNS 共同事業として運営

Shell Evolution Paradigm

Neutron Single-Particle orbits

vs.

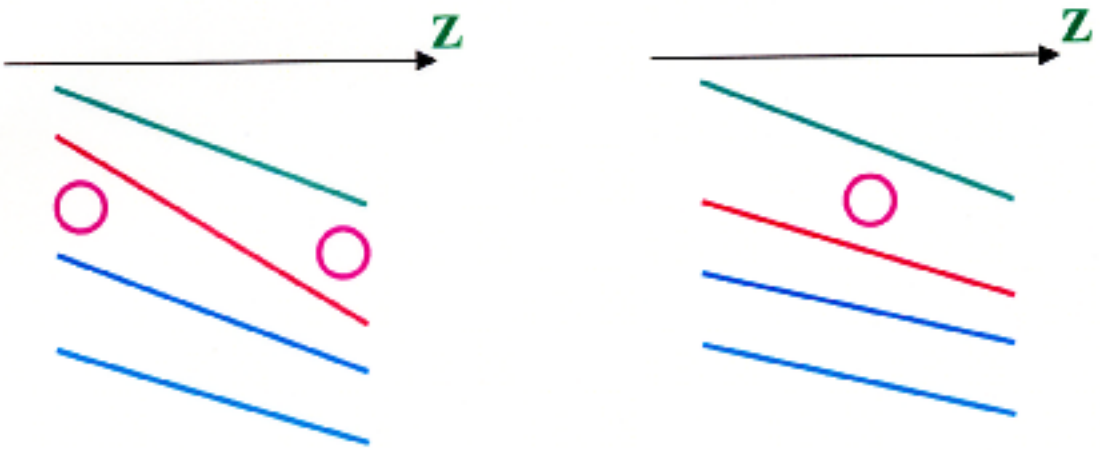

Does the shell structure change without approaching the Drip lines ?

Can the *Nucleon-Nucleon* interaction change the shell structure in a specific way ?

How can we see this shell evolution ?

How general is the shell evolution ?

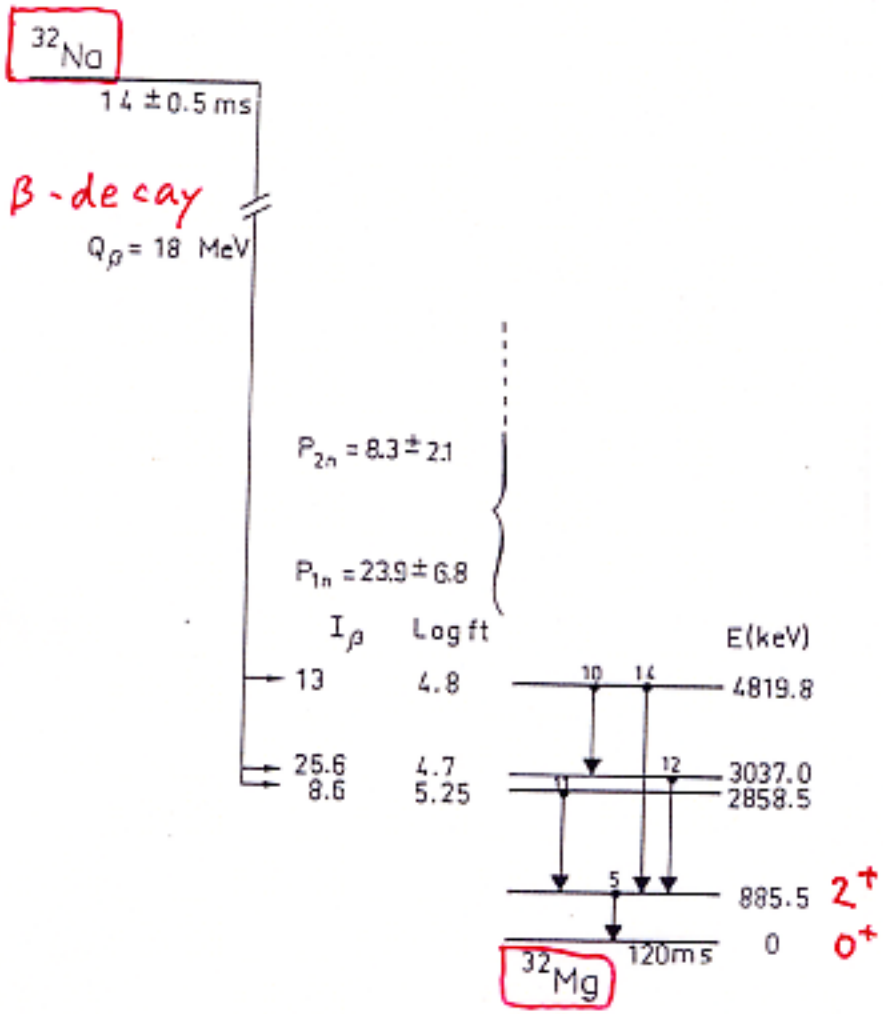

D. Guillemand-Müller et al.

N.P. A426 (84) 37

2^+_1 and 4^+_1 levels and $B(E2; 0^+_1 \to 2^+_1)$

Points : exp Lines : MCSM calc.

● ▲ after calc. —— sd+pf --- sd only

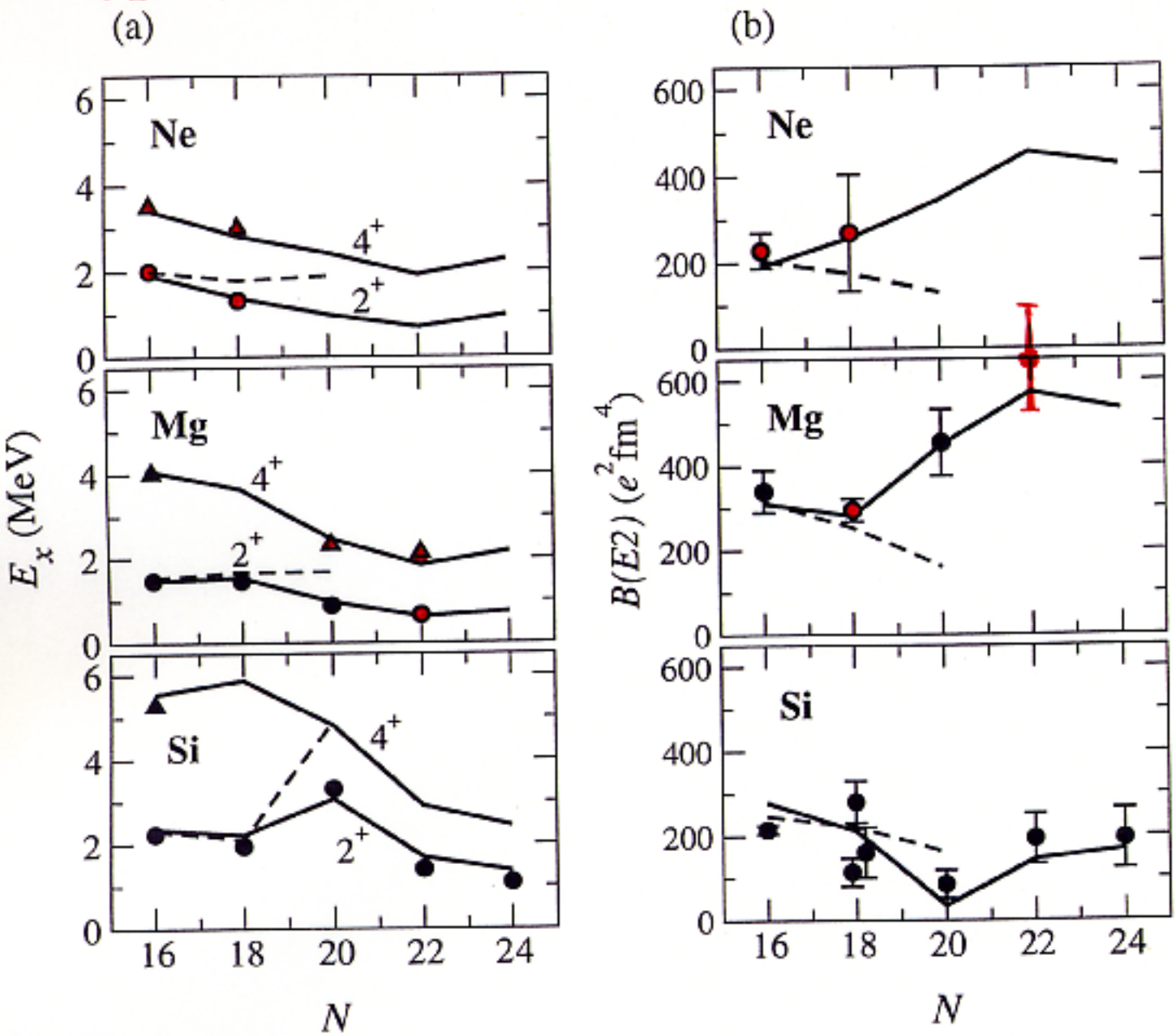

N = 20 isotones

normal configuration

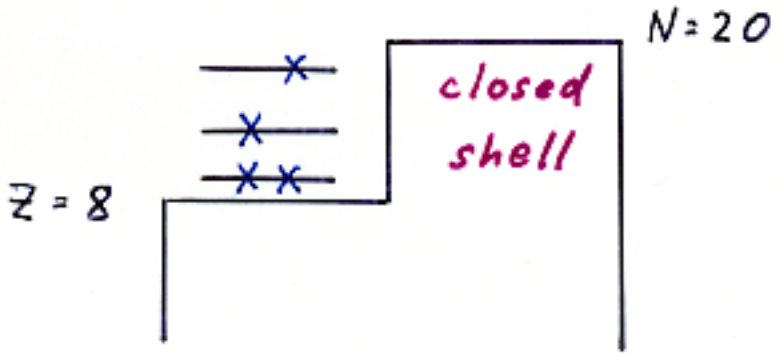

They do mix !

intruder configuration

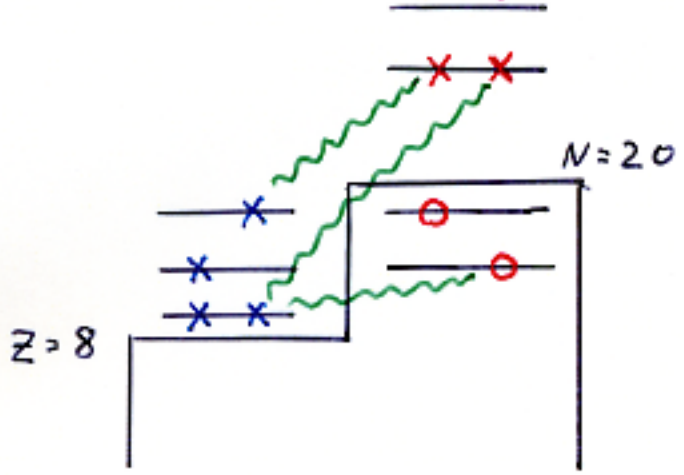

$\Delta\varepsilon_{gap}(Z,N)\Big|_{N=20}$

changes

proton-neutron quadrupole correlation energy

$\sim Q_p\, Q_n$

	Ne	Mg	Si
Q_p	large	largest	modest

Ozawa et al. PRL 84 (2000) 5493

Dlouhý et al NP A701 (2002) 189c

Transition between N = 16 and N = 20 magic schemes

Oxygen isotopes : $^{24}_{8}O_{16}$ is heaviest (Z = 8)

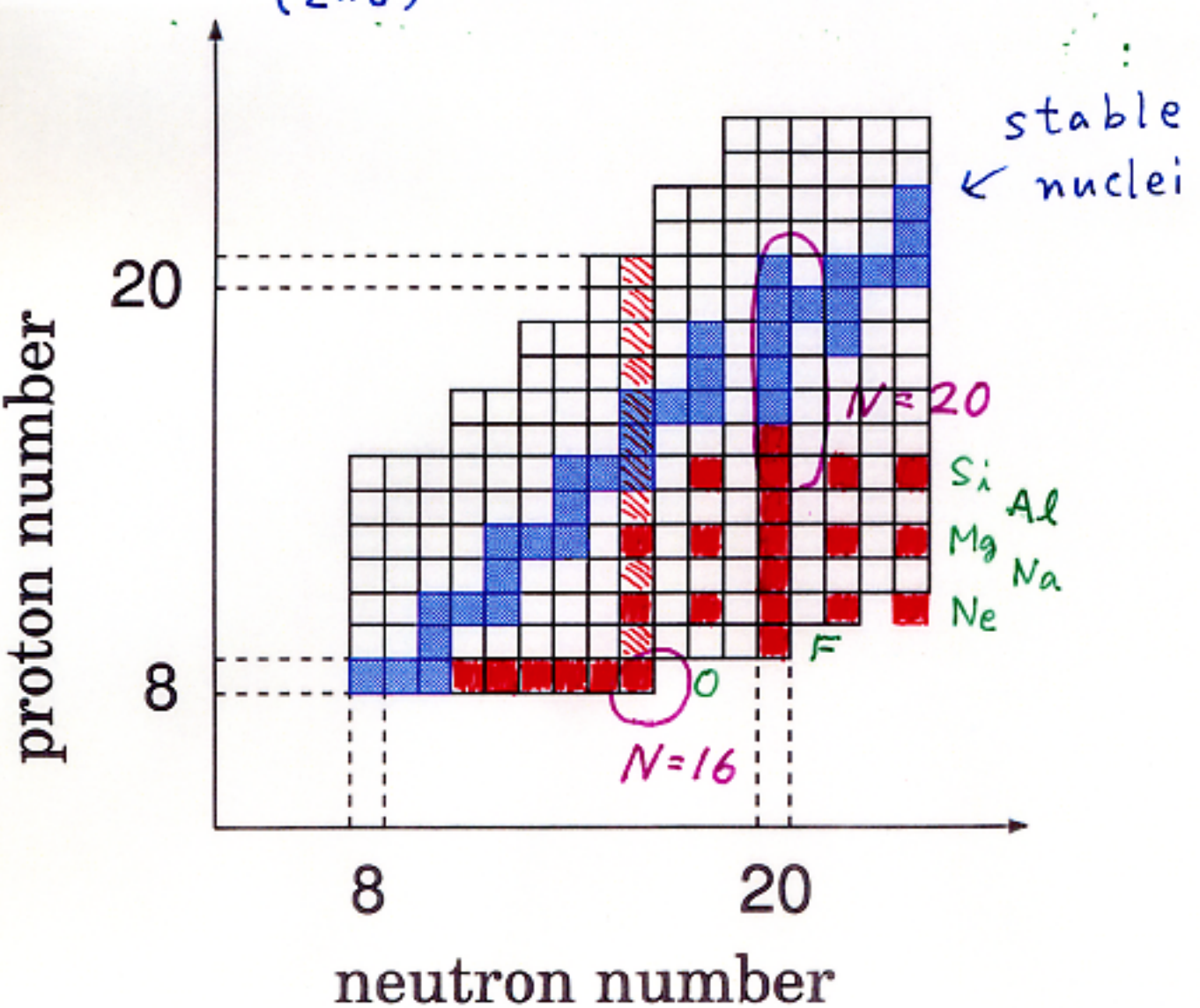

* See also Dlouhý et al. (2001) submitted

$N = 16$: a magic number ?

- Ozawa et al. PRL 84 (2000) 5493
  anomalies in separation-energy systematics for $N \sim 16$ *
- 2^+_1 of ^{24}O and $\frac{3}{2}^+_1$ of ^{25}O in continuum

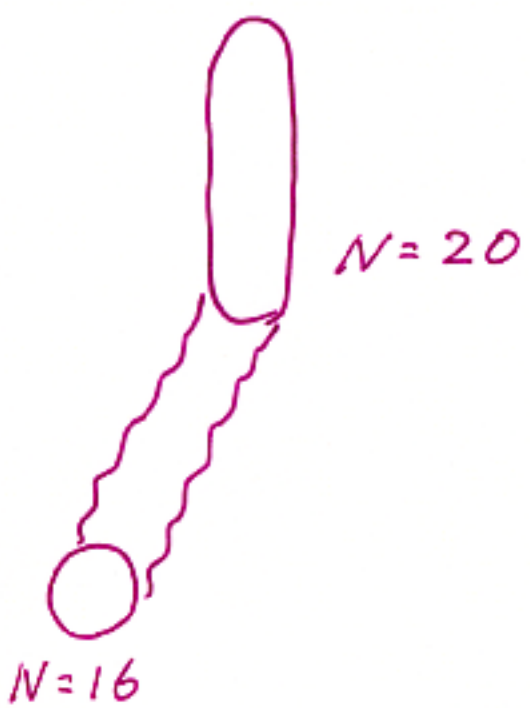

Utsuno, O, et al.
Phys. Rev. C 60
054315 (1999)

Model Space

$1d_{5/2}$, $1d_{3/2}$

$2s_{1/2}$

opposite parity

$1f_{7/2}$

$2p_{3/2}$

Single-particle energies

fixed around ^{40}Ca

Interaction

USD	sd	Wildenthal + Brown 1984
KB	pf	Kuo + Brown 1968
MK'	sd-pf	Millener + Kurath 1975 + Warburton et al. 1986

with the usual $A^{-0.3}$ scaling
for all two-body matrix elements
(adjusted at A=40)

+ additional fine tuning

Oxygen isotopes

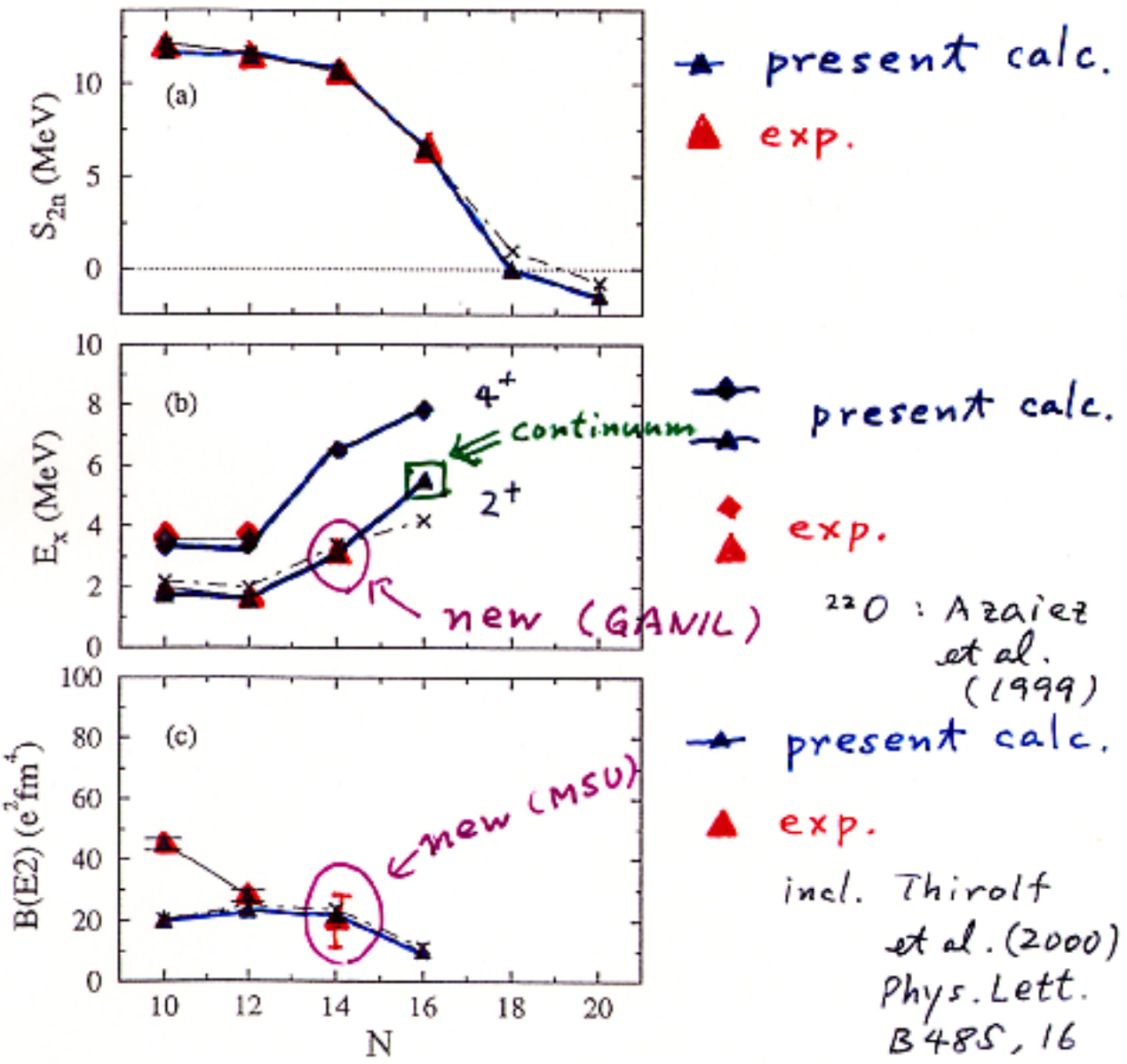

FIG. 3. (a) Two-neutron separation energies, (b) 2_1^+ (triangles) and 4_1^+ (diamonds) levels, (c) $B(E2;0_1^+ \rightarrow 2_1^+)$ values of O isotopes. The filled and open symbols mean the experiment and the calculation by the present interaction, respectively. As a comparison, results by the *sd*-shell model calculation with the USD interaction are shown by the crosses. The 2_1^+ level of ^{22}O is taken from [33].

Effective single-particle energies of neutrons

Oxygen isotopes N=20 isotones

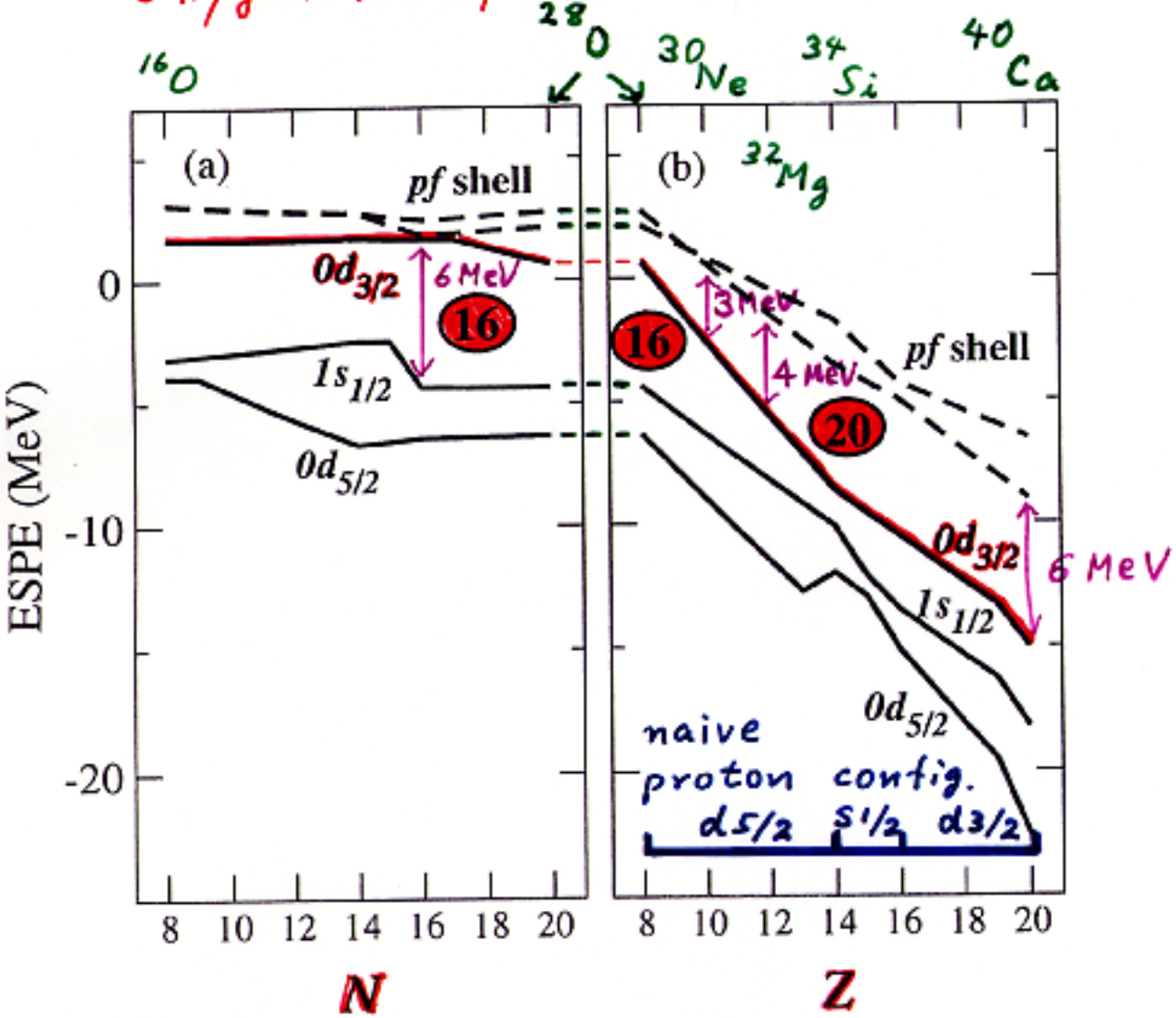

Interaction : sd shell USD (1984)

pf shell Kuo (1968)

sd-pf MK' (1975)
+ Warburton et al (1986)

+ fine tuning Utsuno et al. (1999)

Effective (spherical) single-particle energy, ε_j

- Monopole Hamiltonian

  H' = single particle energy

  + monopole interaction

  $\langle j_1 j_2 : JT | V | j_1 j_2 : JT \rangle$

  This angular momentum dependence is averaged out by a weight $(2J+1)$.

- Using normal filling

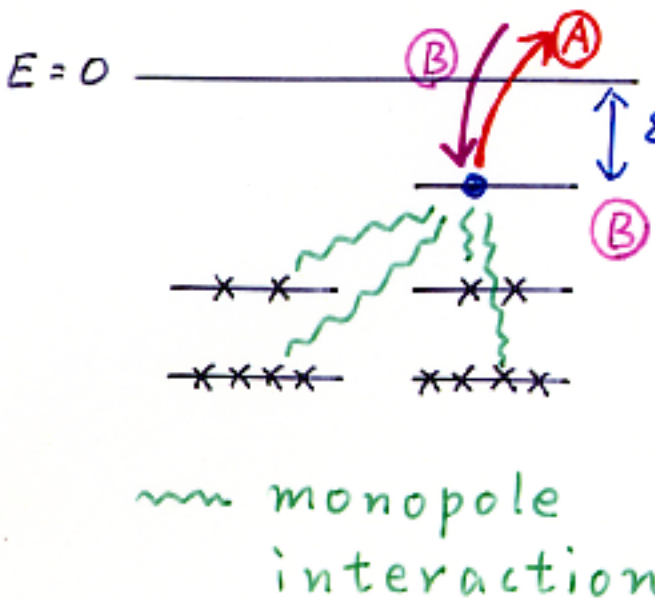

~~~ monopole interaction

Ⓐ for occupied orbit

ε_j = − separation energy (S_n or S_p)

Ⓑ for unoccupied orbit

ε_j = − binding energy gain by putting this nucleon
~~~

Neutron
Effective single-particle Energies
N = 20 isotones

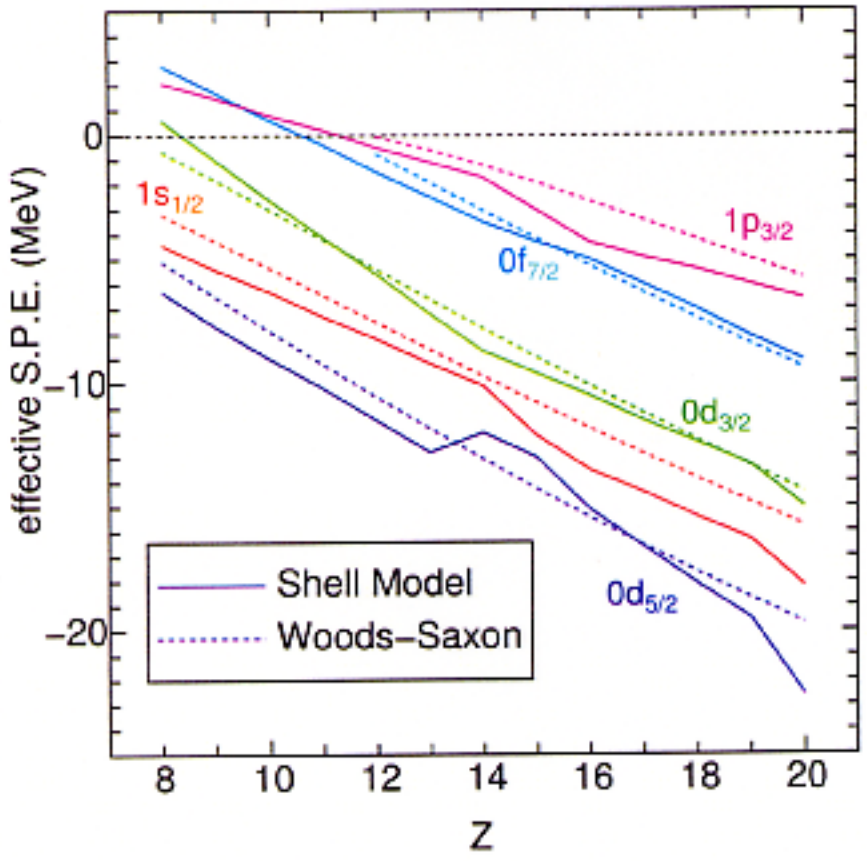

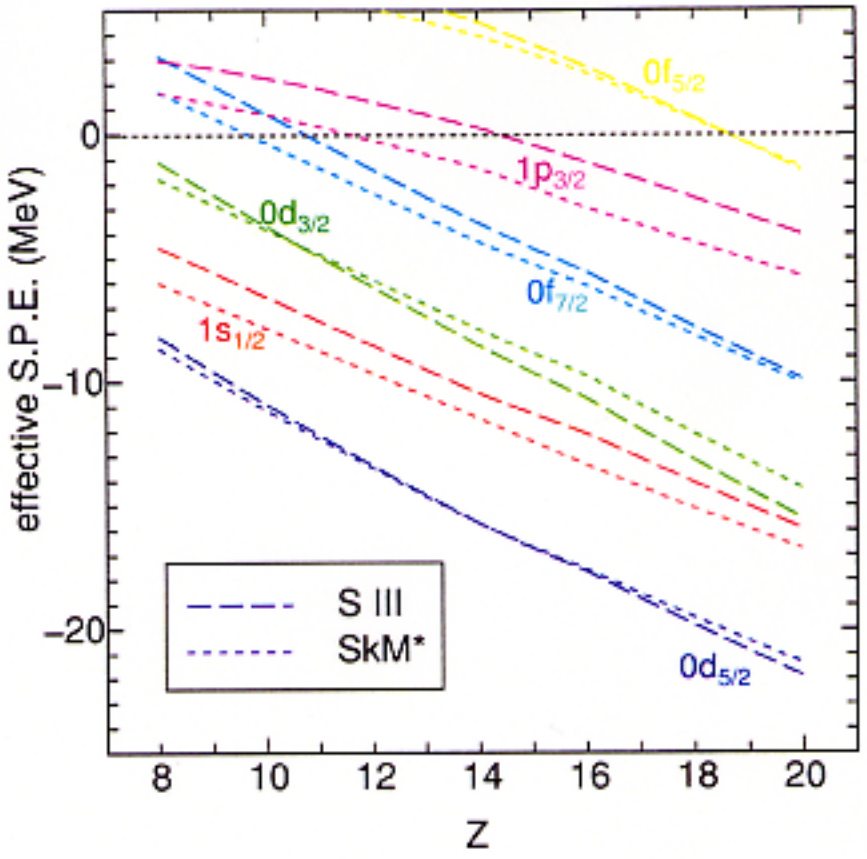

- Strong T=0 attraction in $d_{5/2} - d_{3/2}$ configuration

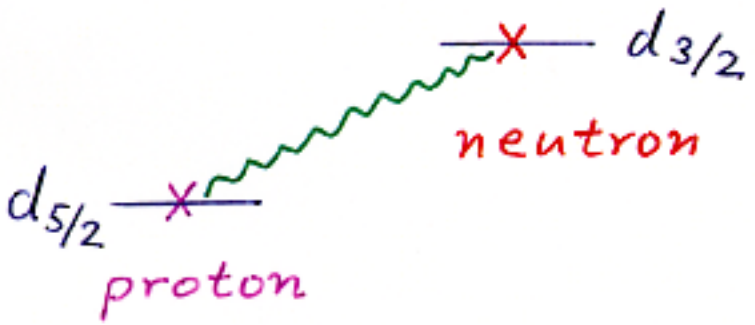

⇒ strong monopole interaction

$^{30}_{14}Si_{16}$

(stable)

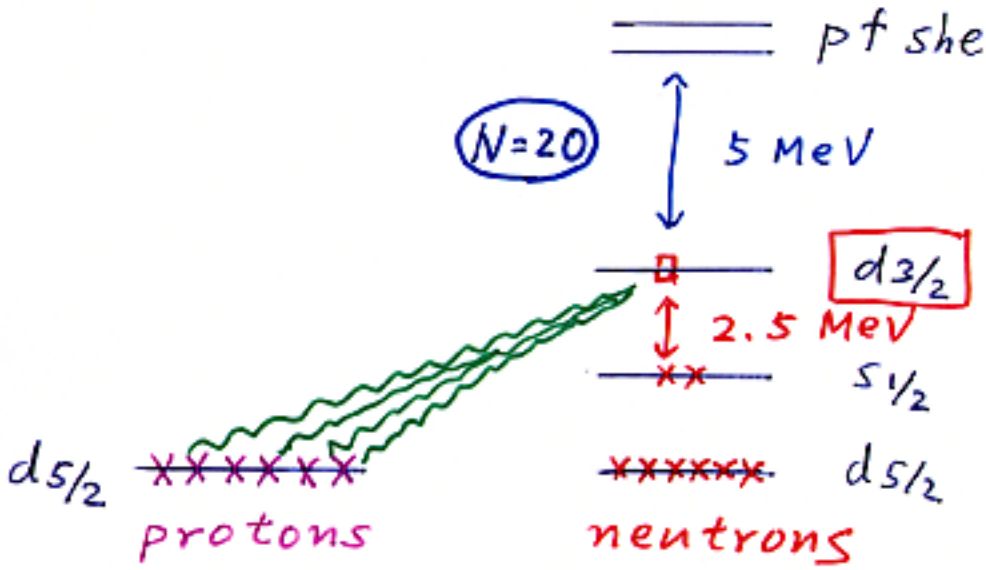

$^{24}_{8}O_{16}$

(unstable)

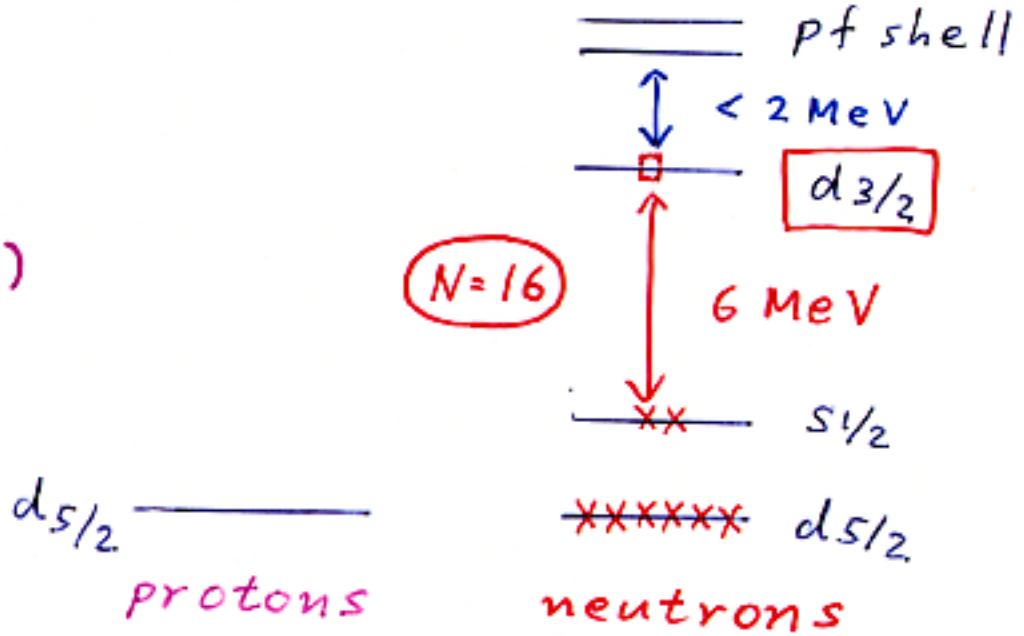

A more general picture

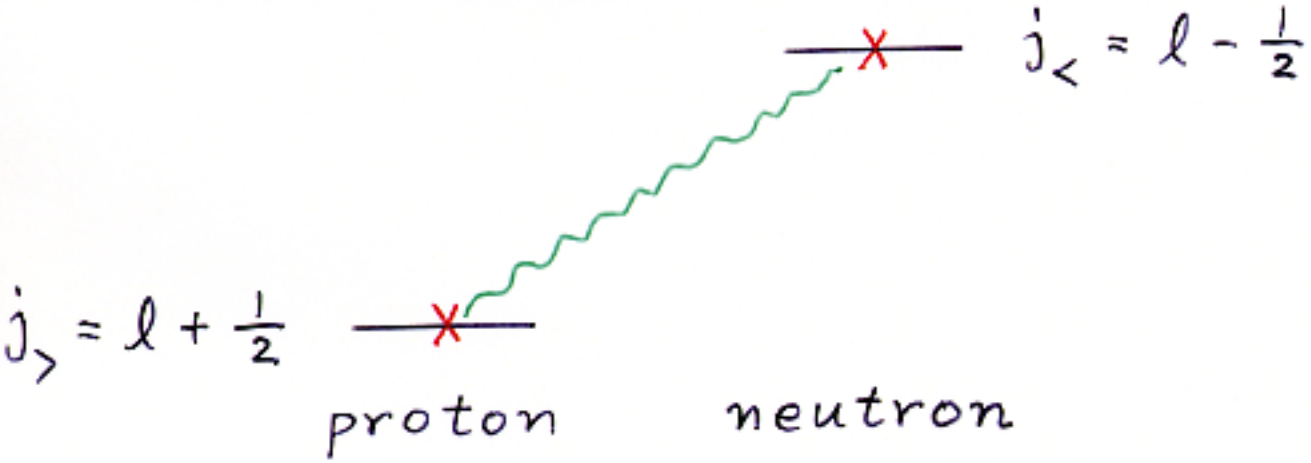

- Strong attractive interaction in $T=0$ channel for $j_> \otimes j_<$ configuration in general

  Ex : $\langle d_{5/2}\ d_{3/2} \mid V \mid d_{5/2}, d_{3/2} \rangle_{J,\ T=0}$
  $p_{3/2}\ p_{1/2}$ $p_{3/2}\ p_{1/2}$

- This interaction contains strong attractive monopole component in general.

  Strongest in one major shell

  - G-matrix p, sd, pf shells
  - USD, GXPF1/2

effective d3/2–s1/2 gap

for neutrons at N=16

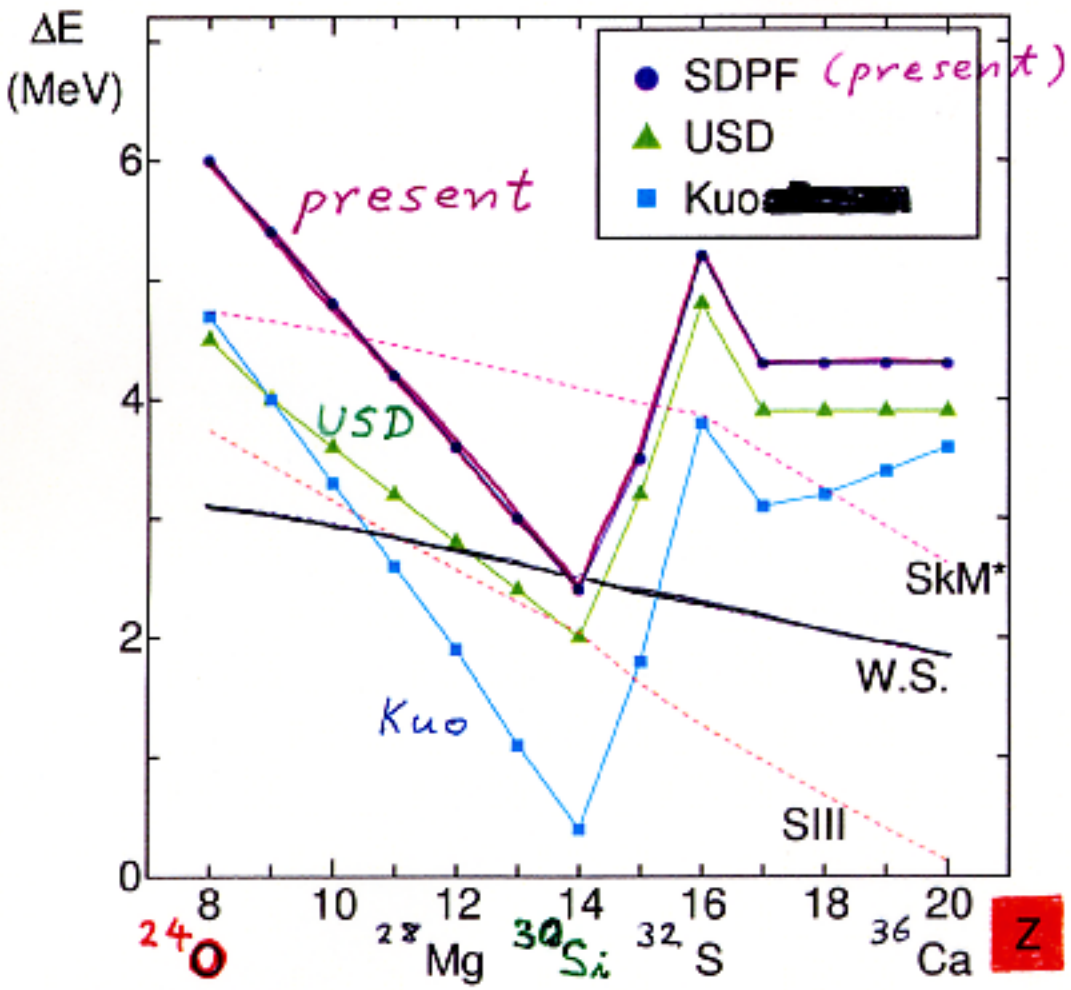

stable

neutron-rich ← → proton-rich

A major mechanism producing this $j_> - j_<$ coupling

$$V_{\tau\sigma} = (\tau\cdot\tau)(\sigma\cdot\sigma) f_{\tau\sigma}(\vec{r})$$

long range limit of $f_{\tau\sigma}(\vec{r})$

$\Rightarrow \overset{\circ}{V}_{\tau\sigma} \propto (\tau\cdot\tau)(\sigma\cdot\sigma)$

This favors

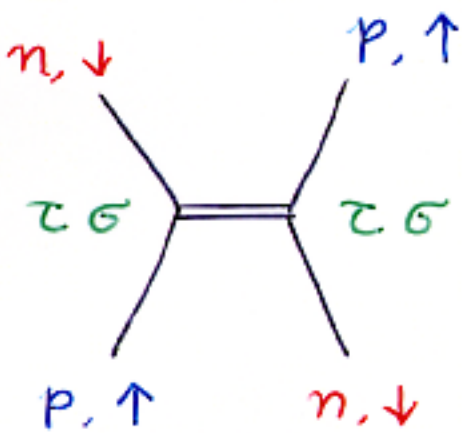

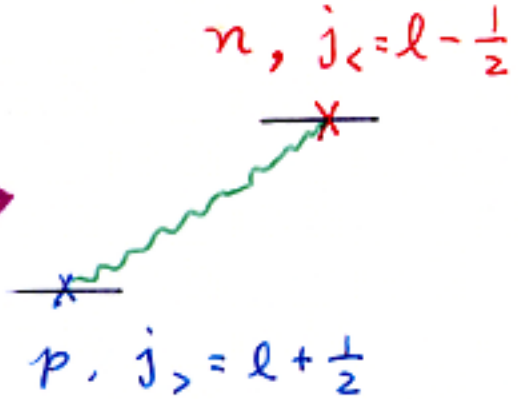

origin in mesons

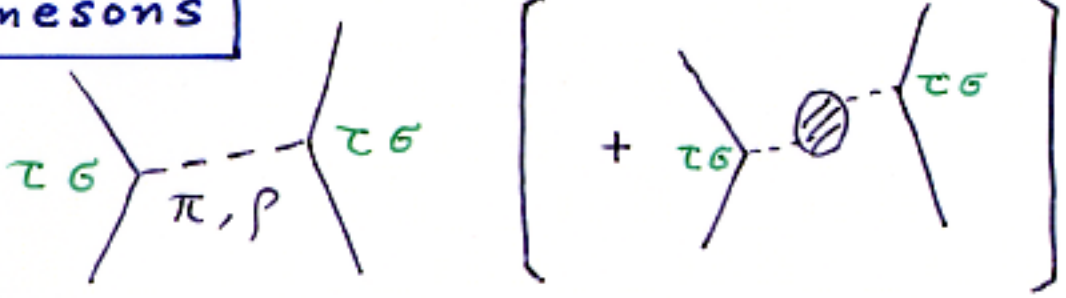

$$V_{OBEP} \propto (\tau\cdot\tau)\{(\sigma\cdot\sigma) + \cdots\} f(r)$$

π : longest range

$$\overset{\circ}{V}_{\tau\sigma} = (\tau\cdot\tau)\,(\sigma\cdot\sigma)$$

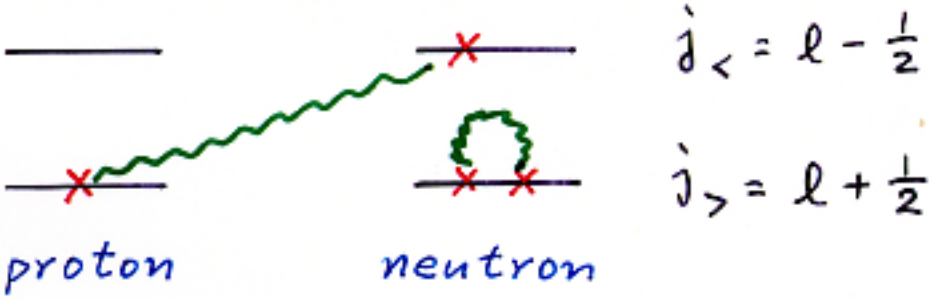

Monopole interaction for $\overset{\circ}{V}_{\tau\sigma}$

$$\frac{\sum_J (2J+1) \langle jj' ; JT | \overset{\circ}{V}_{\tau\sigma} | jj' ; JT \rangle}{\sum_J (2J+1)}$$

j	j'	$T=0$	$T=1$
$\ell+\frac{1}{2}$	$\ell+\frac{1}{2}$	$-\frac{3}{2\ell+1}$	$-\frac{2\ell+3}{(2\ell+1)^2}$
$\ell+\frac{1}{2}$	$\ell-\frac{1}{2}$	$-\frac{6}{2\ell+1}$	$-\frac{2}{2\ell+1}$
$\ell-\frac{1}{2}$	$\ell-\frac{1}{2}$	$-\frac{3(2\ell-1)}{(2\ell+1)^2}$	$-\frac{1}{2\ell+1}$

Relative magnitude for $\ell \gg 1$

j	j'	pn	nn, pp
$\ell+\frac{1}{2}$	$\ell+\frac{1}{2}$	-2	-1
$\ell+\frac{1}{2}$	$\ell-\frac{1}{2}$	$\boxed{-4}$	-2
$\ell-\frac{1}{2}$	$\ell-\frac{1}{2}$	-2	-1

$_{11}Na$ isotopes

^{31}Na spectrum

Quadrupole and Magnetic moments

Na isotopes

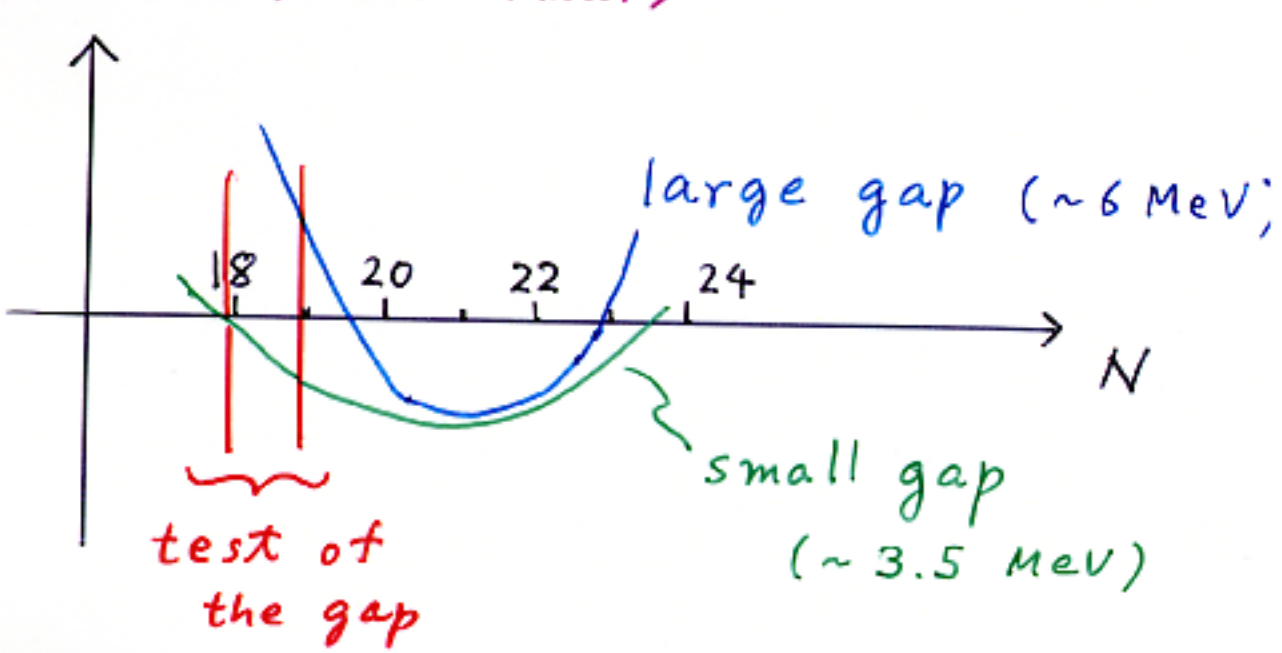

- At $N=20$, the correlation energy is minimum for normal state because of neutron closed shell.
- At $N=22$, the deformation energy becomes largest.

Present Hamiltonian ⇒ small gap for Na

Utsuno et al PRC 60, 054315 (1999)

sd + $f_{7/2}$ $p_{3/2}$

good for F, Ne, Na, ···, Al. Ar

Na isotopes

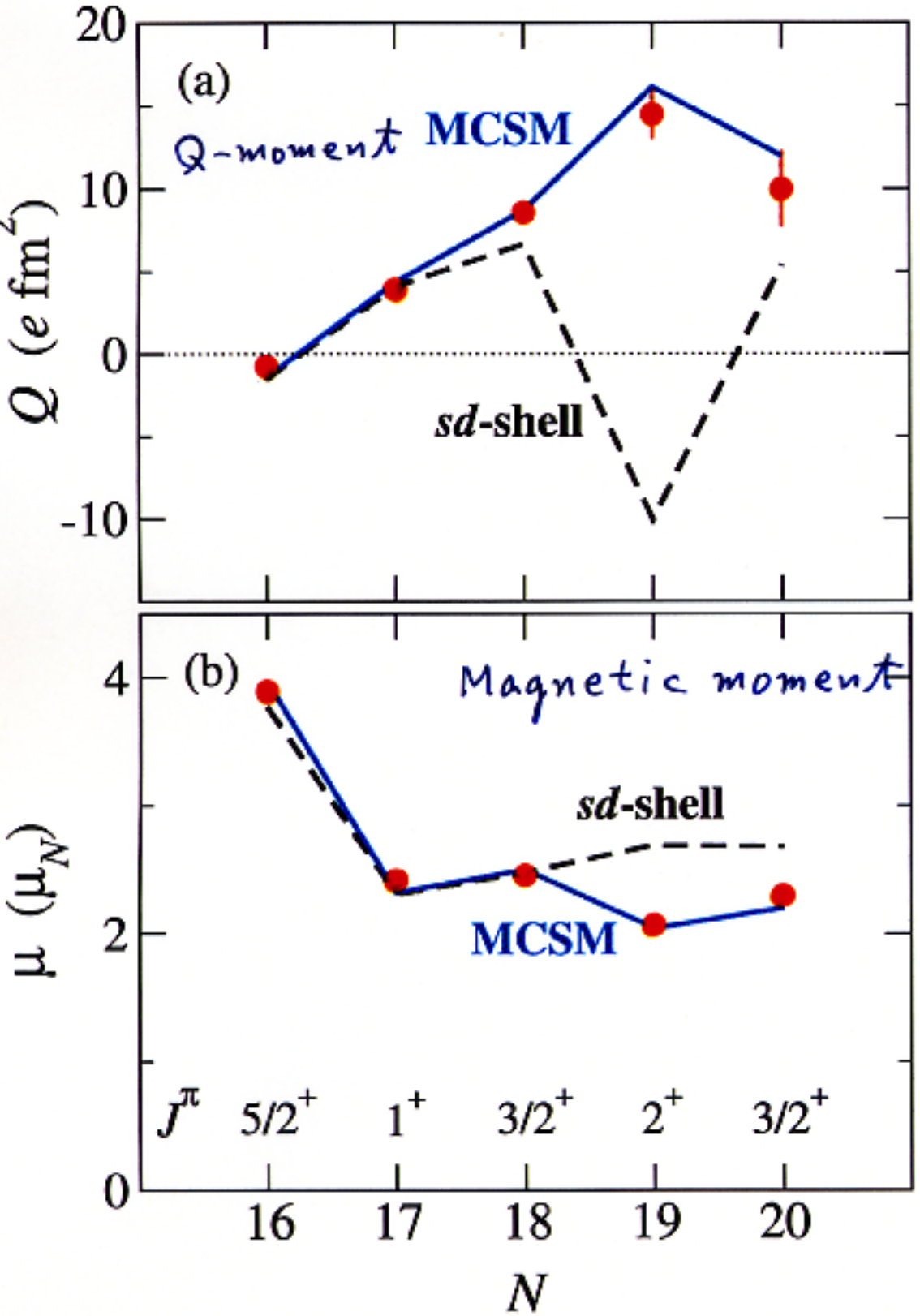

Ref.) M. Keim *et al.*, in *Proc. of "Exotic Nuclei and Atomic Masses" (1998)*; Eur. Phys. J A **8**, 31 (2000).

Ground-state configurations in Na

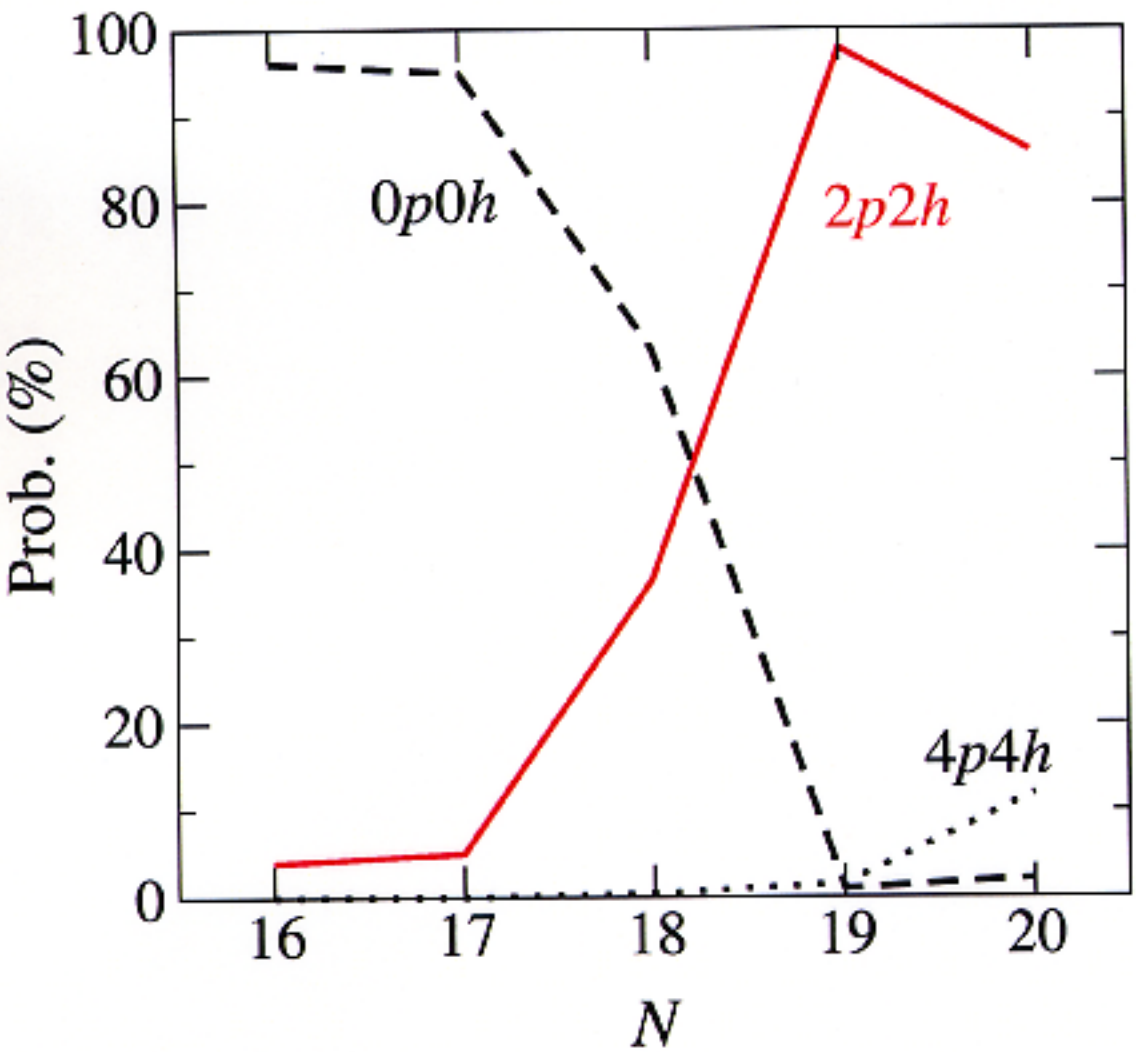

Exp. Prytychenko et al.
MSUCL 1233 (2002); Phys. Rev. C

$B(E2; 2^+ \to 3^+)$ $130 \pm {}^{90}_{65}$ (e^2fm^4)

168 (e^2fm^4)
present calc. (MCSM)

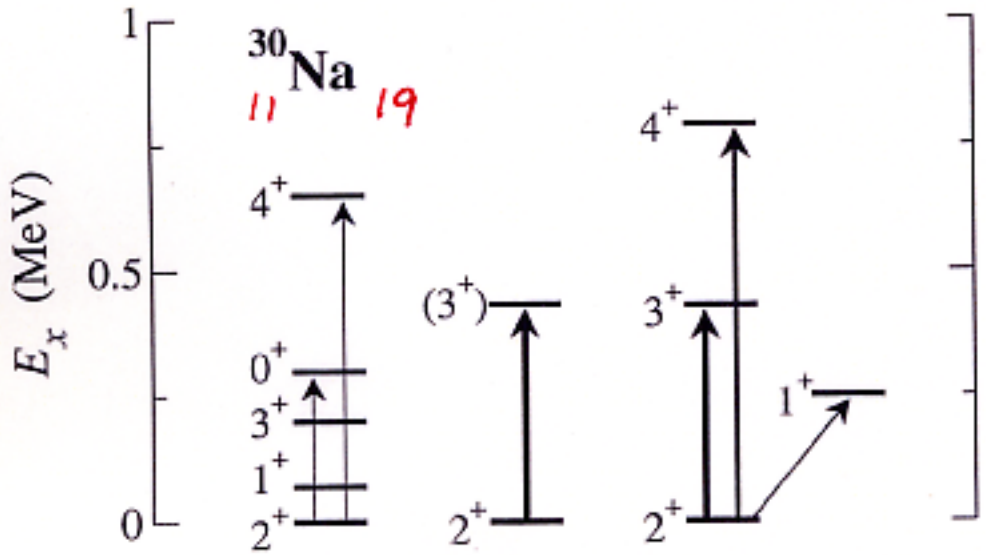

↑
normal states only

↑
sd + pf
2^+ : intruder

Shape Evolution of Exotic Mg Isotopes

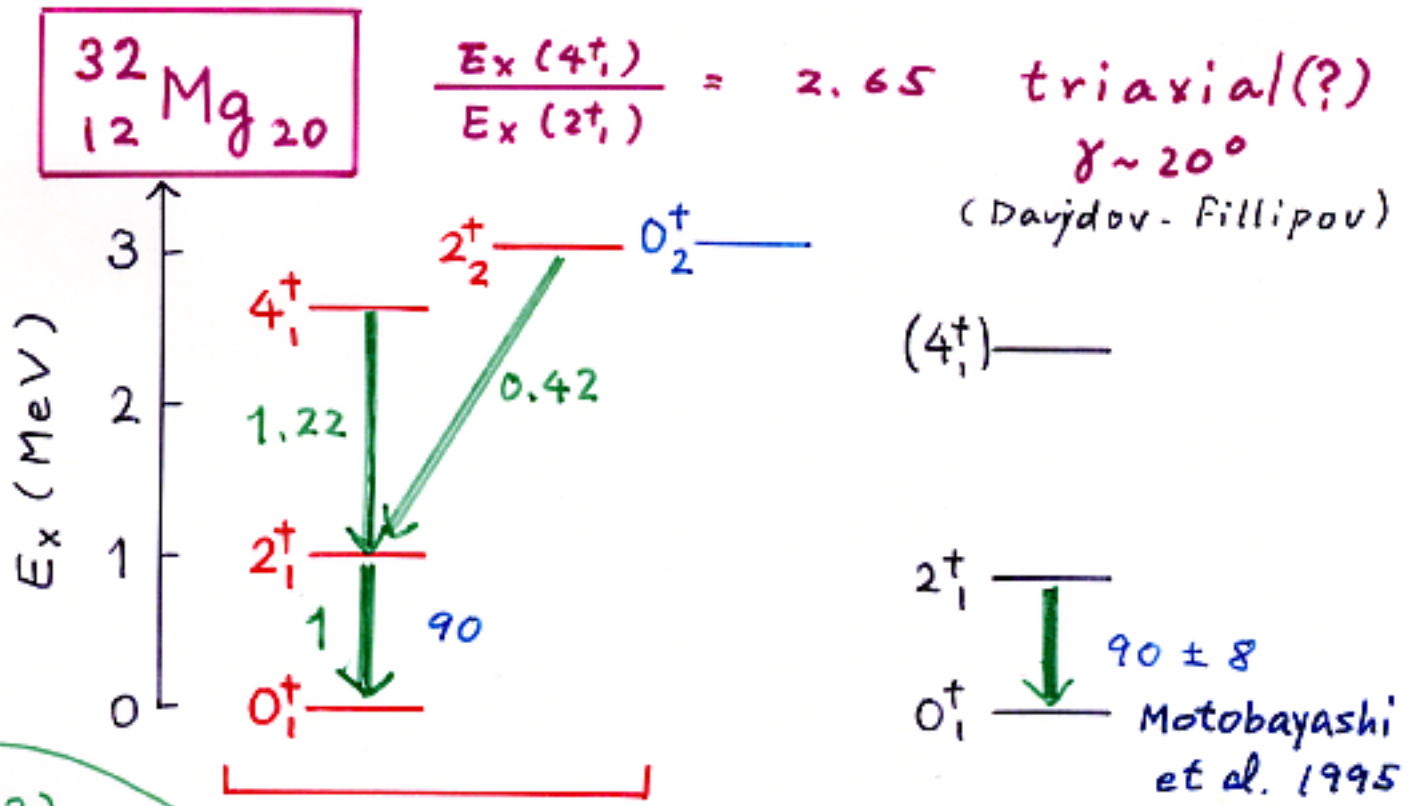

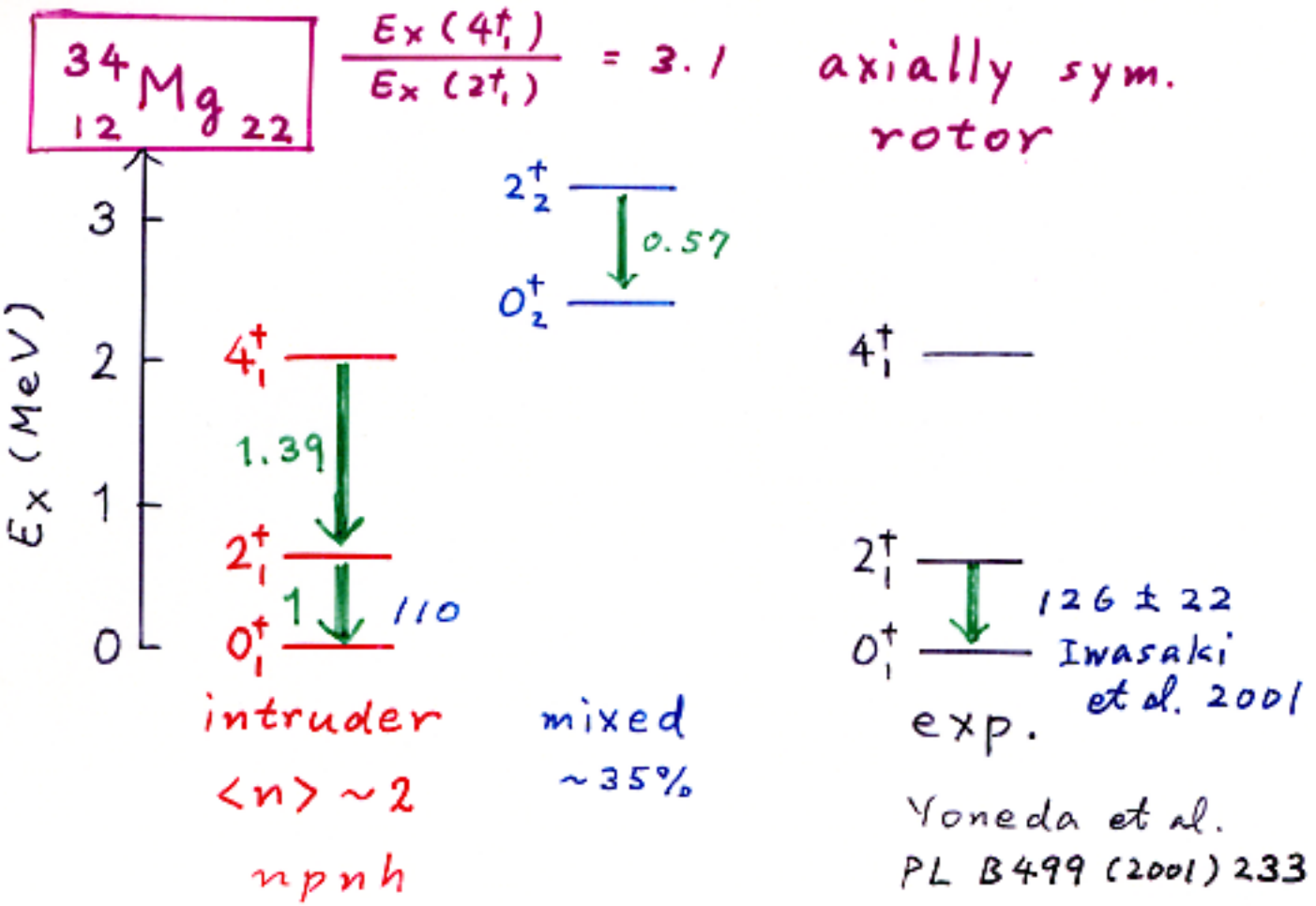

ISSN 1343-2230
CNS-REP-38
ISSN 1346-244X
RIKEN-AF-NP-409
October, 2001

CNS

CNS Report

Large collectivity of ^{34}Mg

H. Iwasaki, T. Motobayashi, H. Sakurai, K. Yoneda,
T. Gomi, N. Aoi, N. Fukuda, Zs. Fülöp, U. Futakami,
Z. Gacsi, Y. Higurashi, N. Imai, N. Iwasa, T. Kubo,
M. Kunibu, M. Kurokawa, Z. Liu, T. Minemura, A. Saito,
M. Serata, S. Shimoura, S. Takeuchi, Y. X. Watanabe,
K. Yamada, Y. Yanagisawa, and M. Ishihara

submitted to Physics Letters B

Center for Nuclear Study (CNS)

Graduate School of Science, the University of Tokyo
Wako Branch at RIKEN, Hirosawa 2-1, Saitama 351-0198, Japan
Correspondence: cnsoffice@cns.s.u-tokyo.ac.jp

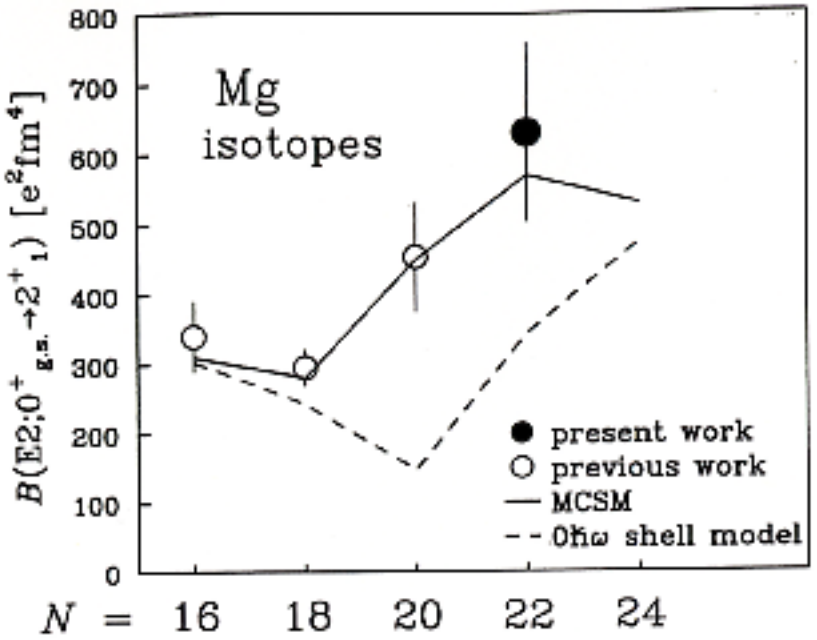

FIG. 3. Measured $B(E2;0^+_{g.s.} \rightarrow 2^+_1)$ values for ^{28}Mg [30], ^{30}Mg [28], and ^{32}Mg [8] as well as the present result on ^{34}Mg are compared with two shell model calculations. Predictions by the Monte Carlo shell model (MCSM) [13] and the 0ħω shell model calculation in Ref. [12] are indicated by the solid and dashed lines, respectively.

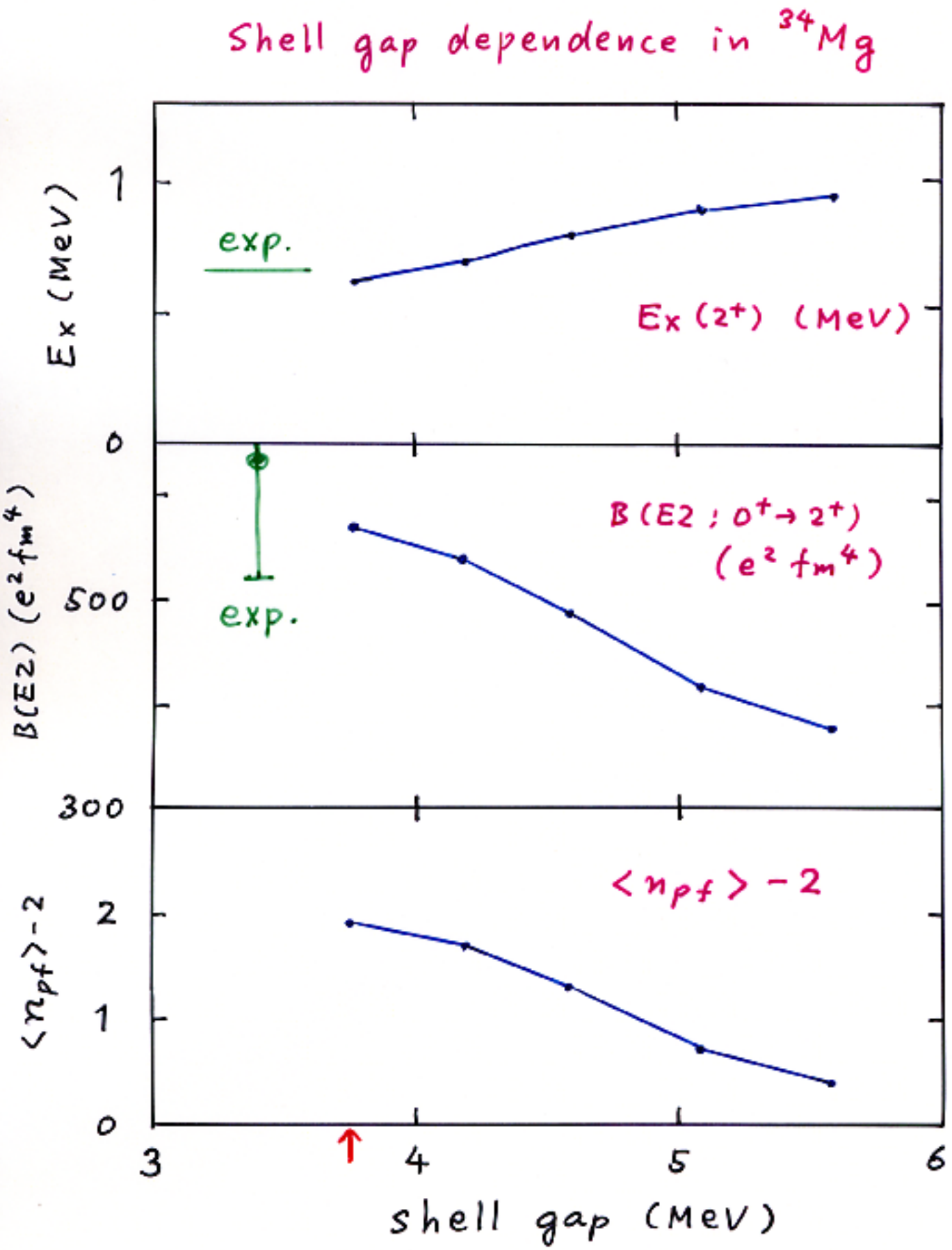
Shell gap dependence in ^{34}Mg
Ex (MeV)
1
0
exp.
Ex (2+) (MeV)
B(E2) (e²fm⁴)
500
300
exp.
B(E2 ; 0+ → 2+)
(e² fm⁴)
<npf> -2
2
1
0
3
4
5
6
shell gap (MeV)
present

Potential Energy Surface for various values of the Shell Gap at N=20

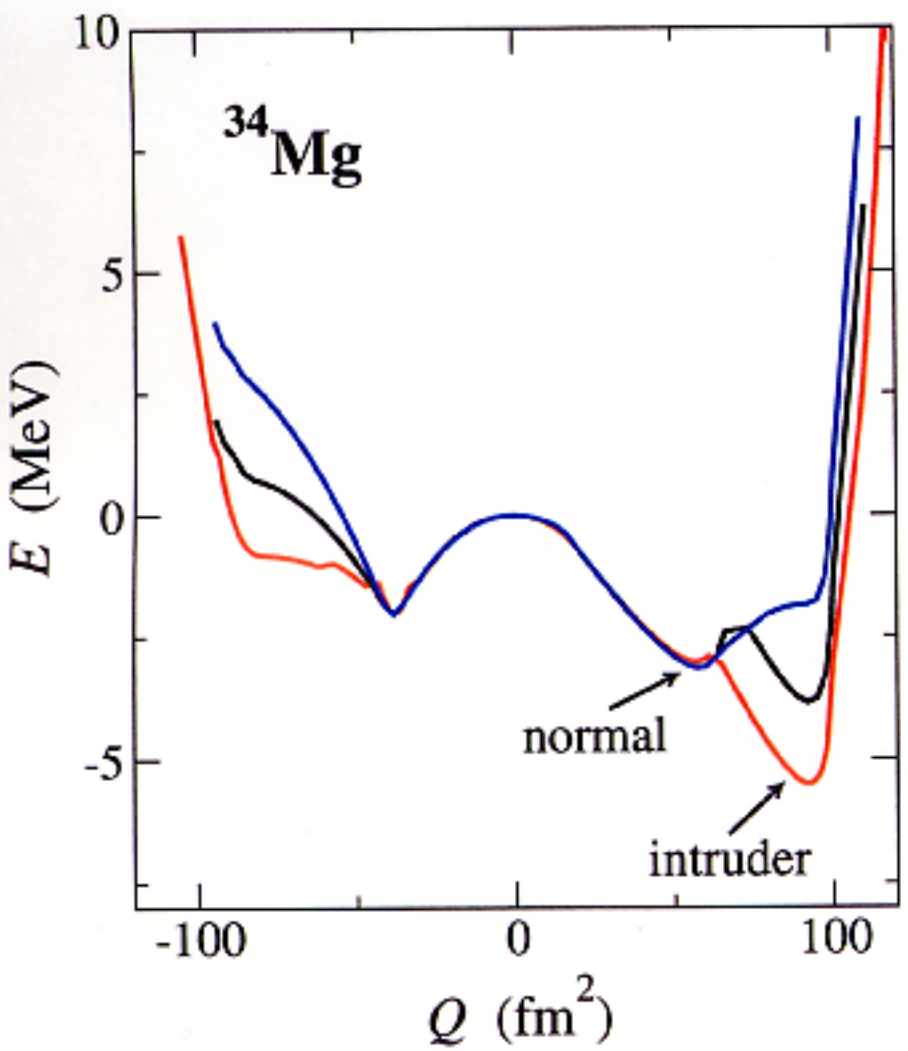

Shell Gap

— 3.8 MeV *

— 4.6 MeV

— 5.6 MeV

* Gap obtained from the present Hamiltonian

$N = 34$ magic structure

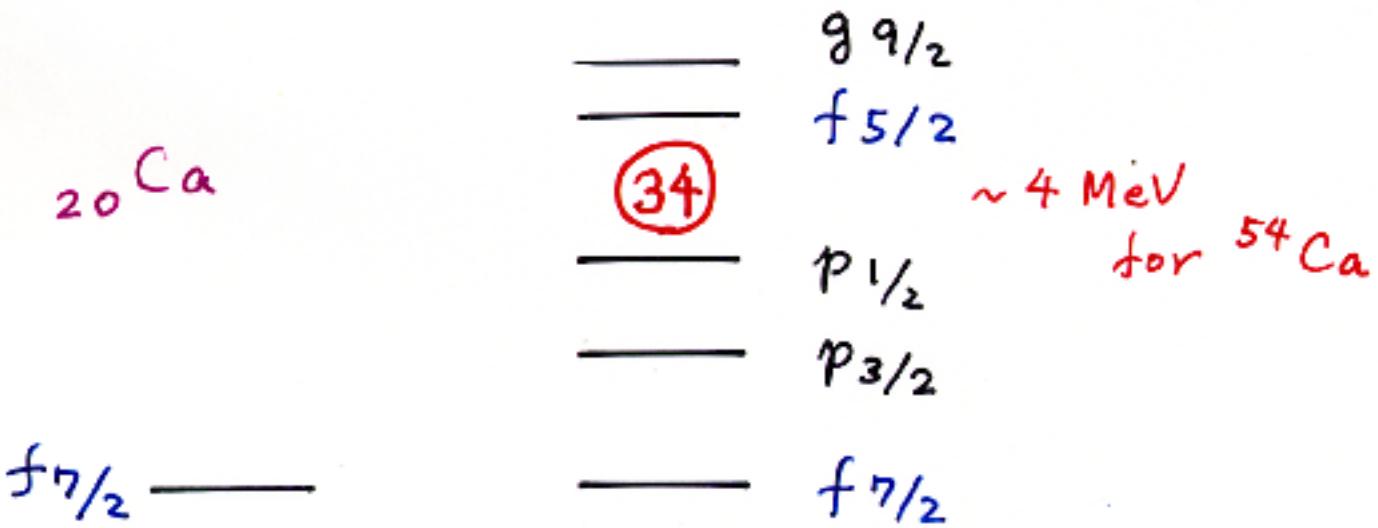

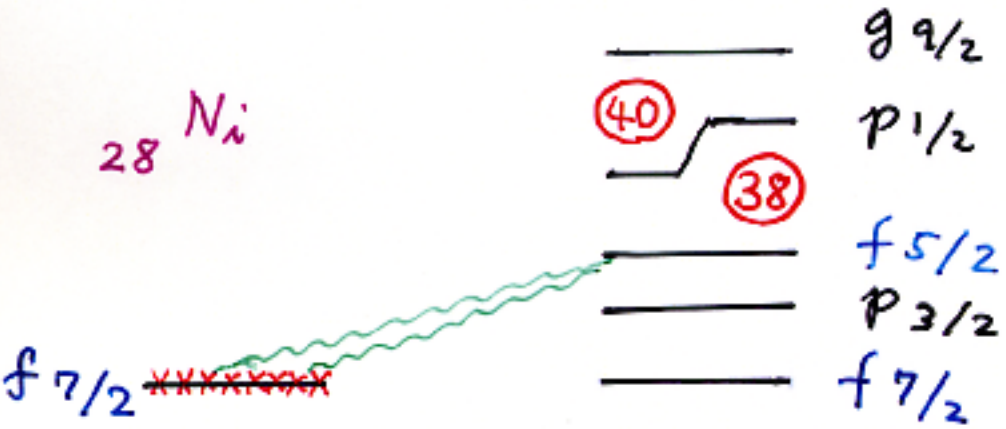

Note : A new effective interaction

GXPF1 (2) by Honma et al.

➪ strongest attractive

diagonal matrix elements

are for $|f_{7/2} \otimes f_{5/2}; J, T=0\rangle$

New effective interaction GXPF1/2

- effective interaction for full pf-shell calculations

  p shell Cohen-Kurath 1965

  sd shell Wildenthal-Brown 1988

- 195 two-body matrix elements

  4 (bare) single particle energies

- G-matrix with core polarization correction by Hjorth-Jensen

  ⇨ starting point

- χ^2-fit

  70 (or 60) best determined linear combinations

  ⇕

  699 (623) data from 87 nuclei (^{47}Ca ~ ^{65}Ge)

  699 = 490 yrast + 198 yrare + 11 higher

- rms error 168 (188) keV

  for mass, ~130 keV

Energy Levels of ^{56,57,58}Ni

Full pf-shell calculation by MCSM

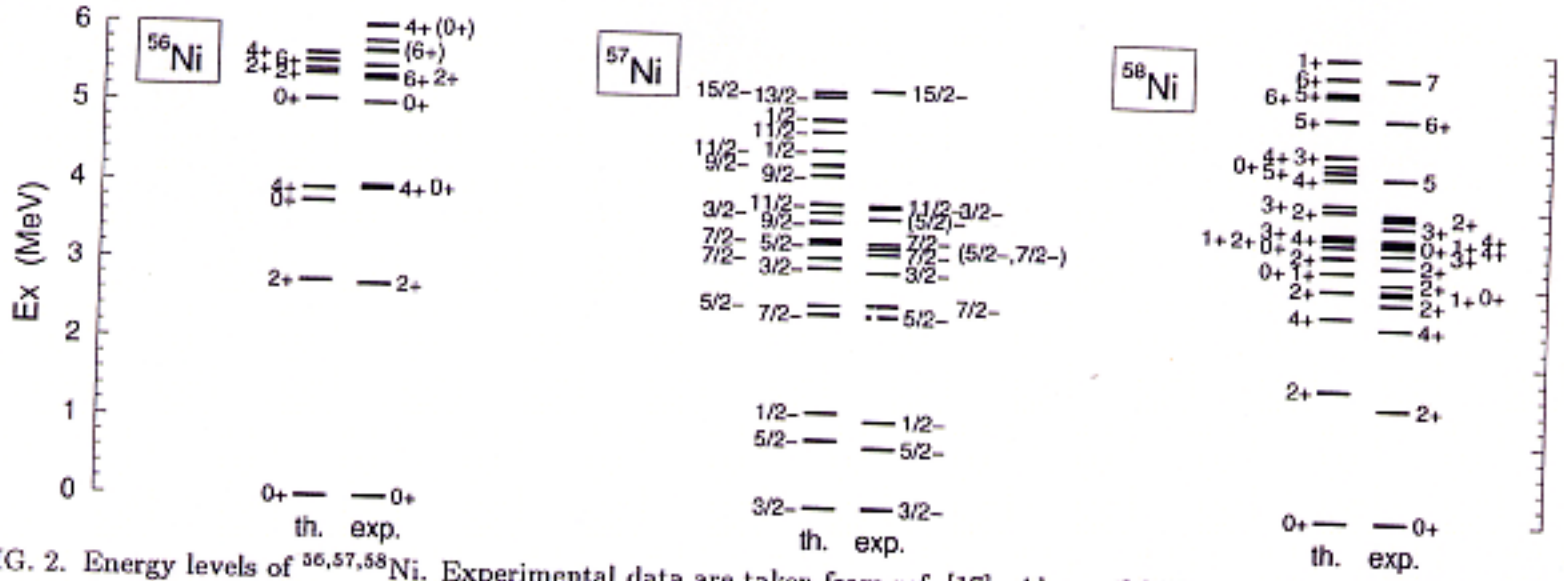

FIG. 2. Energy levels of ^{56,57,58}Ni. Experimental data are taken from ref. [17]. Above 4MeV, experimental levels are shown only for yrast states for ^{57,58}Ni.

GXPF1 interaction

Honma et al.

Phys. Rev. C65, 061301(R) (2002)

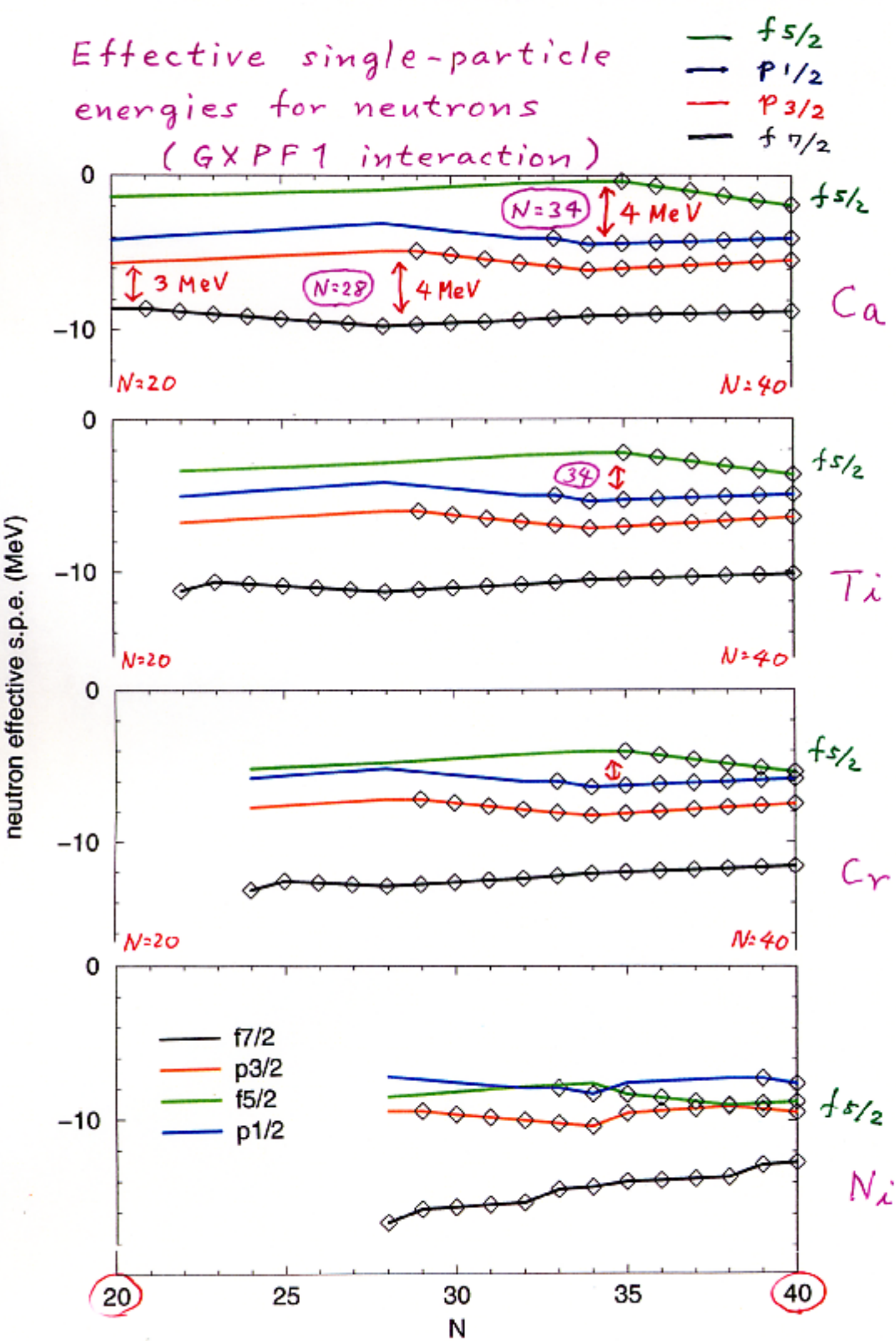
Effective single-particle energies for neutrons
(GXPF1 interaction)
f5/2
p1/2
p3/2
f7/2
N=34
4 MeV
3 MeV
N=28
4 MeV
Ca
N=20
N=40
34
Ti
Cr
Ni
f7/2
p3/2
f5/2
p1/2
neutron effective s.p.e. (MeV)
0
−10
20
25
30
35
40
N

Full pf-shell calculations
with GXPF1 interaction

2^+ levels eff. s.p.e's

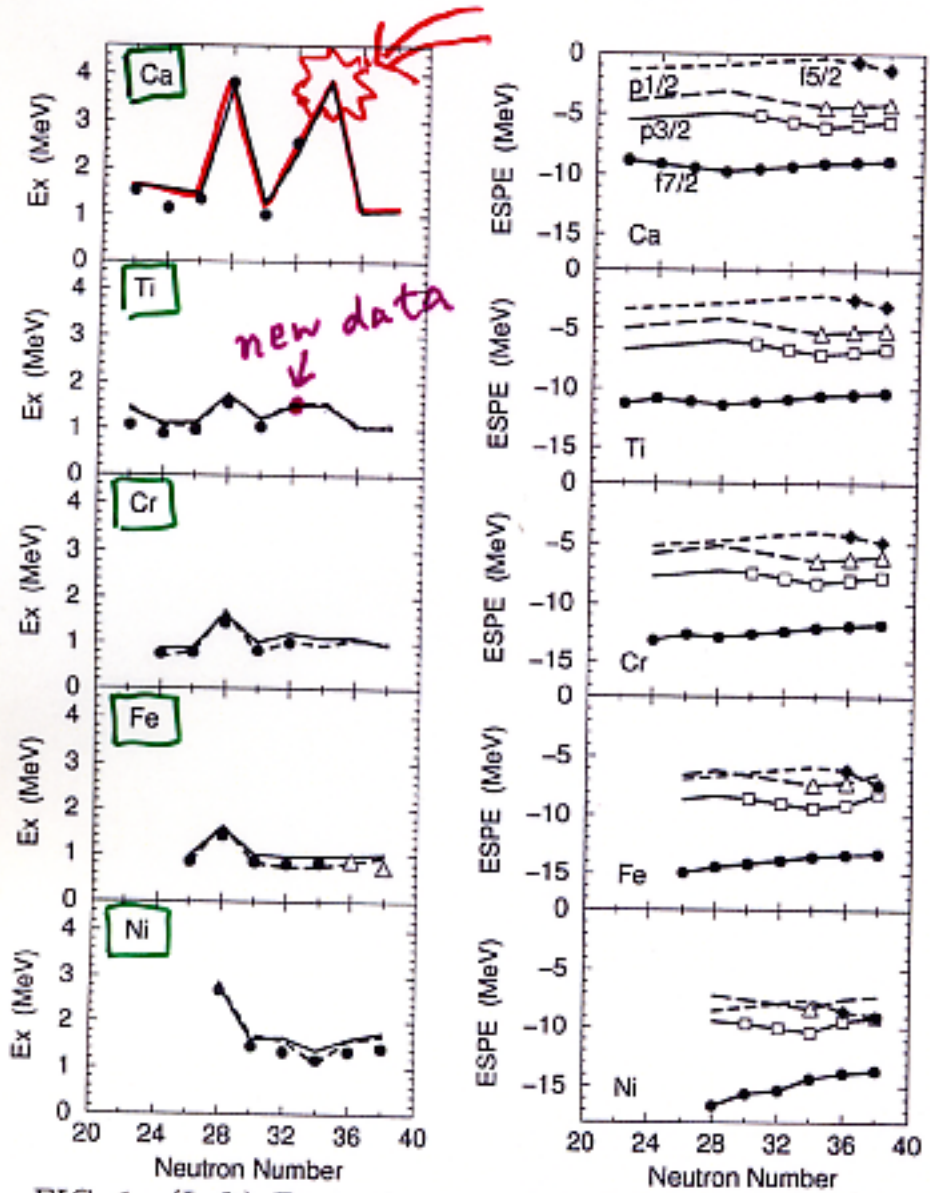

FIG. 1. (Left) Excitation energies of the first 2^+ states. Experimental data are shown by filled circles [17] and open triangles [18]. Theoretical values obtained by shell model calculations are shown by solid lines. The truncation order t (the maximum number of nucleons which are allowed to excite from $f_{7/2}$ to higher orbits: $p_{3/2}$, $p_{1/2}$, $f_{5/2}$) is 5 for ^{56}Fe and ^{58,60,62}Ni, 6 for ^{52,54}Fe and ^{56}Ni, and 7 for ^{58,60}Fe. Other results are exact. Dashed lines show the results obtained by the FDA*. (Right) Effective single particle energies for neutron orbits. Symbols indicate that the corresponding orbit is occupied by at least one nucleon in the lowest filling configuration.

Honma et al.
Phys. Rev.
C65, 061301(R)
(2002)

pf-shell interactions
(2-body matrix elements)

GXPF1 : empirically determined
two-body interaction

vs.

G-matrix with core-polarization
corrections from Bonn-C (H.-Jensen)

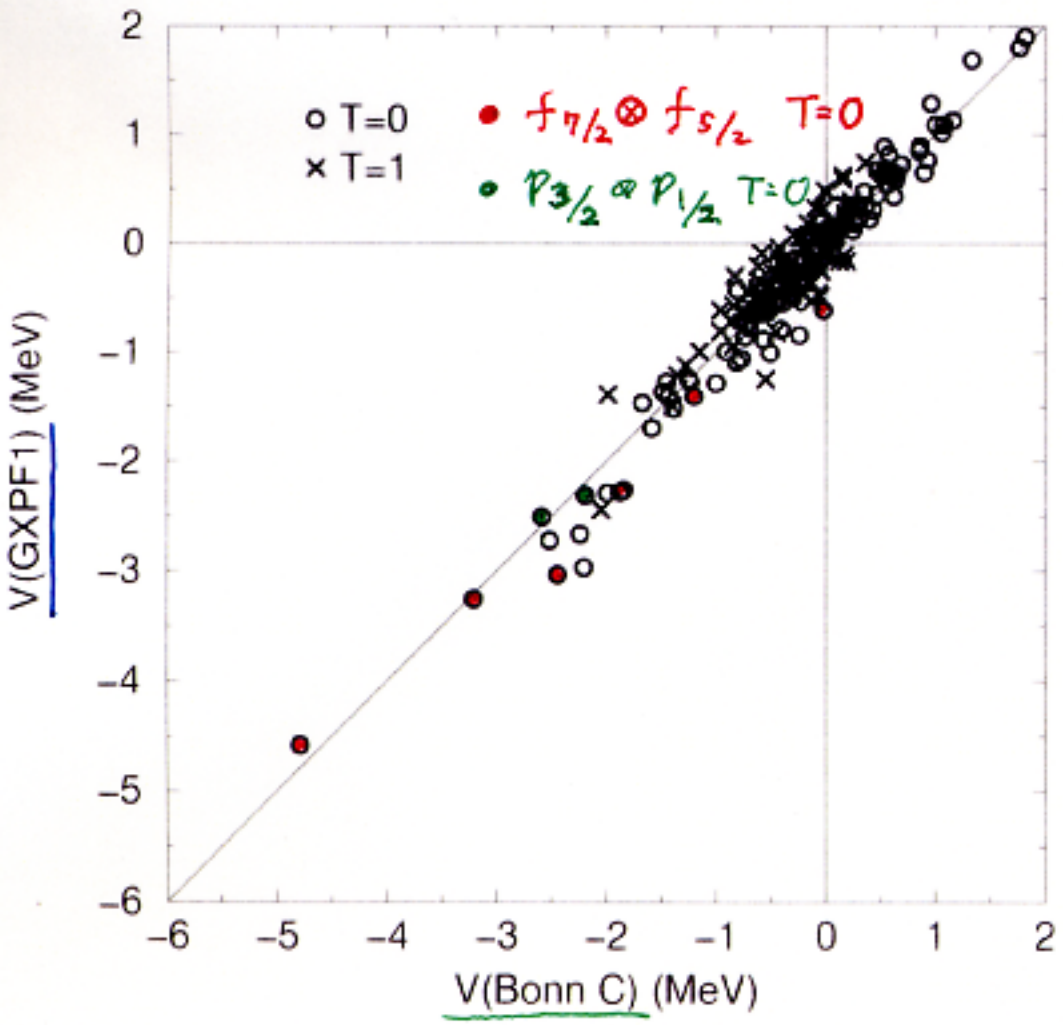

R.V.F. Janssens et al. (2002)

22 Ti

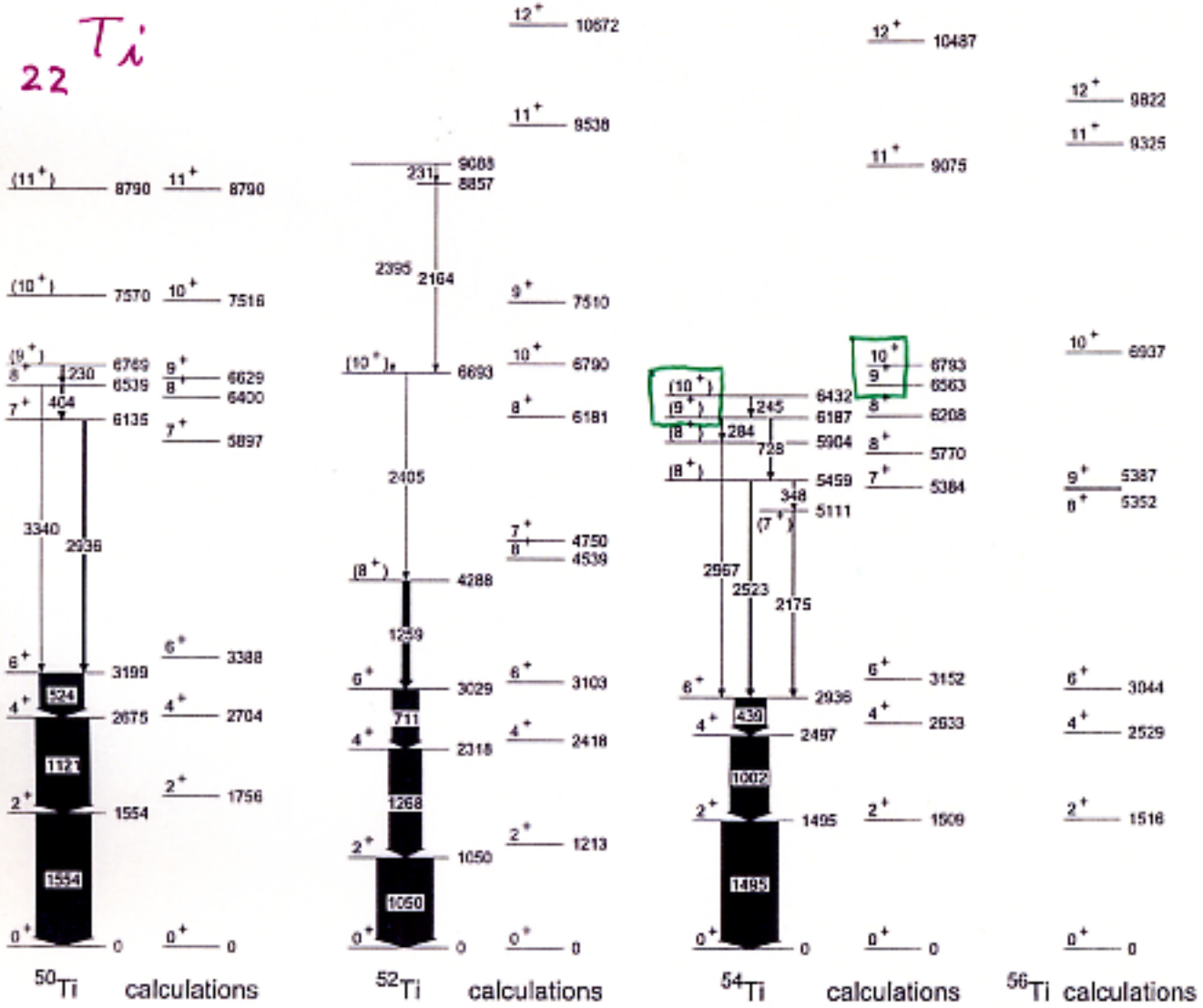

N = 28 30 32 34

calc.
=
gxpf1 int.

$7^+, 8^+$

$\sim \pi (f_{7/2})^2 \quad J_p = 6$

$\otimes \nu (p_{3/2})^3 (p_{1/2}) \quad J_n = 2$

$9^+, 10^+$

$\sim \pi (f_{7/2})^2 \quad J_p = 6$

$\otimes \nu (p_{3/2})^3 (f_{5/2}) \quad J_n = 3, 4$

$N = 8 \rightarrow 6$

stable exotic

in p shell

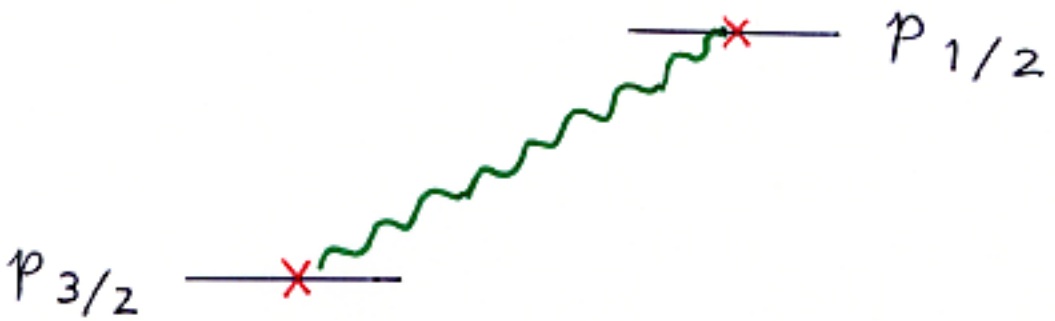

proton neutron

Modification of Shell-model Hamiltonian

Starting from psdmk2 (CK)

CK : Cohen-Kurath
N.P. 73, 1 (65)

Bare single particle energies
on top of the ^{4}He core

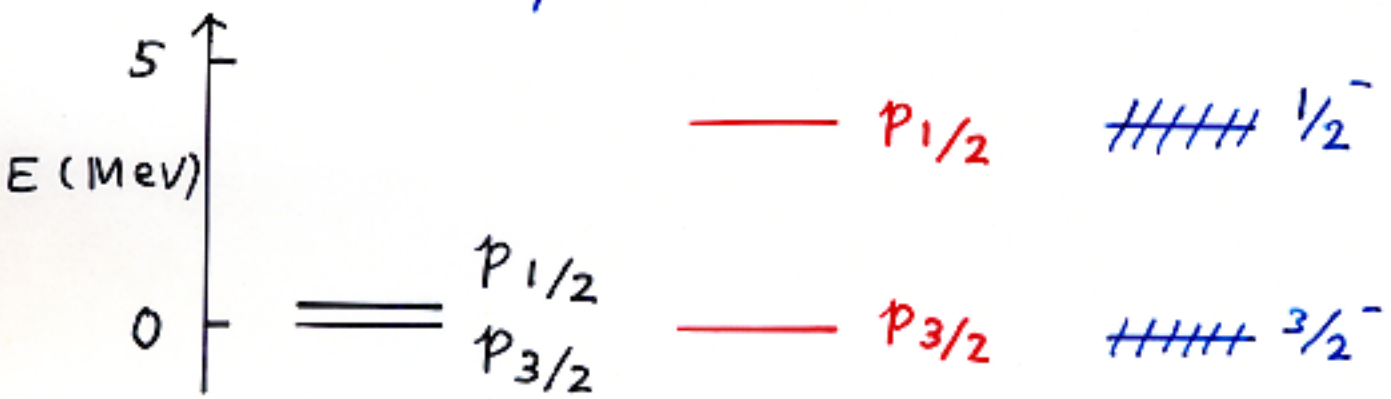

Two-body matrix elements (MeV)
(diagonal ones)

	J	T	psdmk2 (CK)	present	G-matrix (H.-Jensen)
$p_{3/2} \otimes p_{1/2}$	1	0	-6.22	-8.22	-10.02
	2	0	-4.00	-6.00	-9.41

⇧
monopole 2MeV stronger
than psdmk2

Cohen-Kurath vs. Present Interactions

$N \sim Z$ nuclei

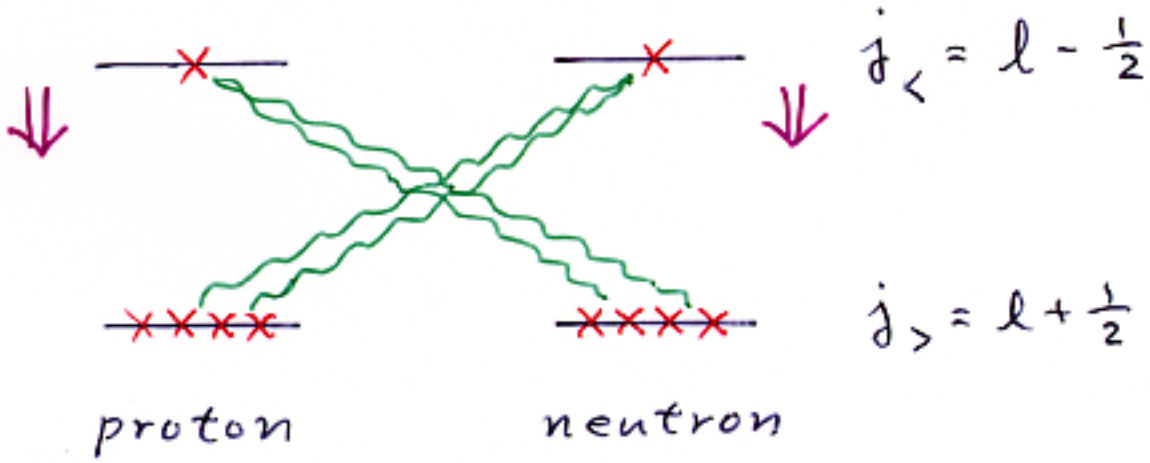

high $\varepsilon(j_<)$ + strong $V_{j_> - j_<}$

present

$\approx$

low $\varepsilon(j_<)$ + weak $V_{j_> - j_<}$

Cohen-Kurath

$N \gg Z$ or $N \ll Z$

no such similarity

Energy Levels of ^{13}C, ^{11}Be & ^{9}He relative to experimental ground state

$^{13}_{6}C_{7}$ stable

$^{11}_{4}Be_{7}$ unstable

^{9}He unstable (unbound)

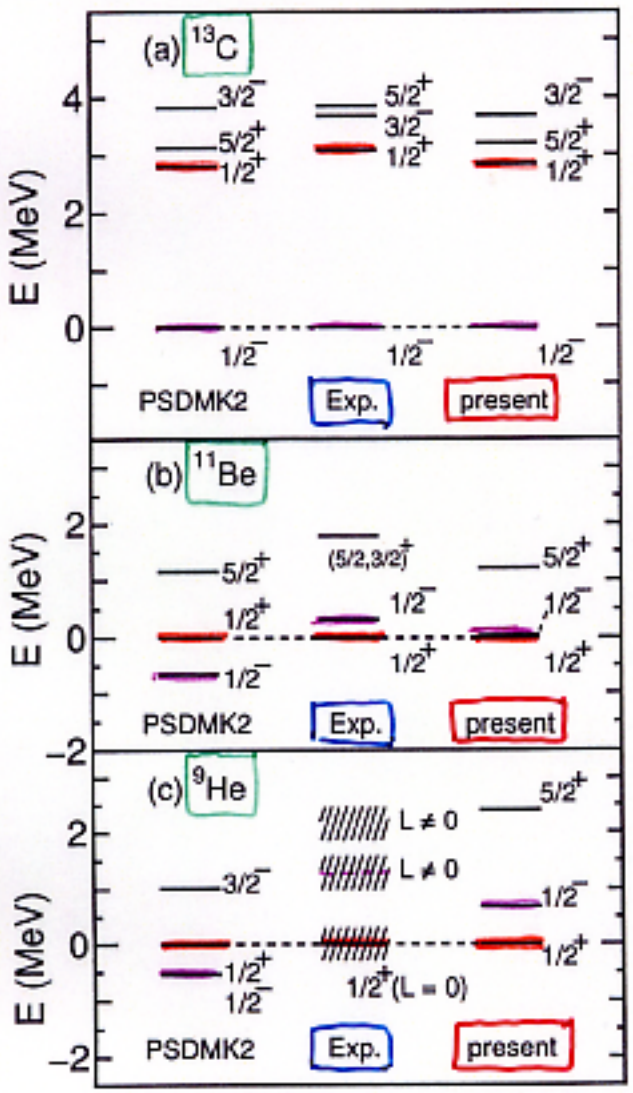

PSDMK2 Exp. Present Calc.

spin and GT properties are preserved or improved

S-factor of $2S_{1/2}$ in the $(1/2)_1$ state ~ 75%

- magnetic mom. Neugart et al.
- Transfer reaction Fortier et al.
- B(GT: $3/2^-$ (^{11}B) → $1/2^-$ (^{11}Be)) Ohnishi et al.

Effective single-particle energy of $1p_{1/2}$ relative to $2s_{1/2}$

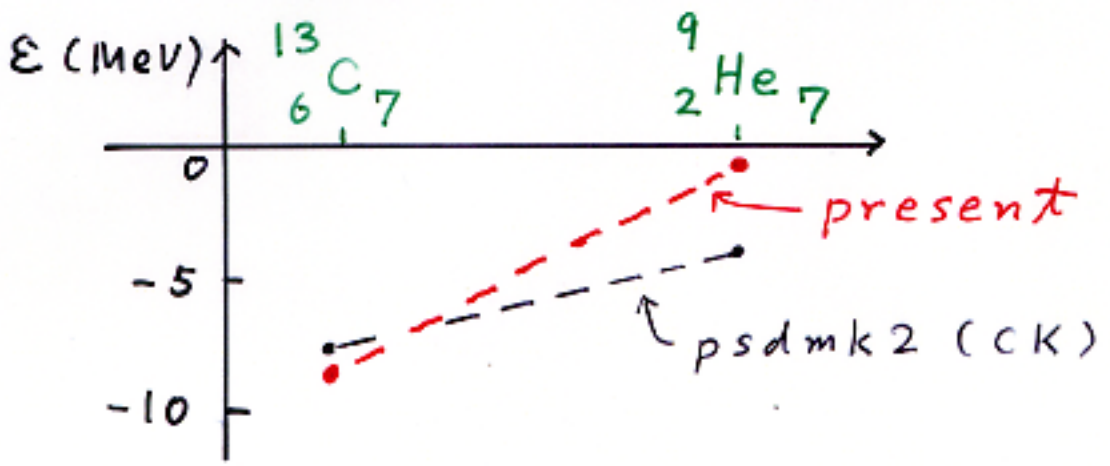

$1s_{1/2} - 0p_{1/2}$ shell gap

$^{12}_{4}Be_{8}$

4.5 MeV 6.5 MeV

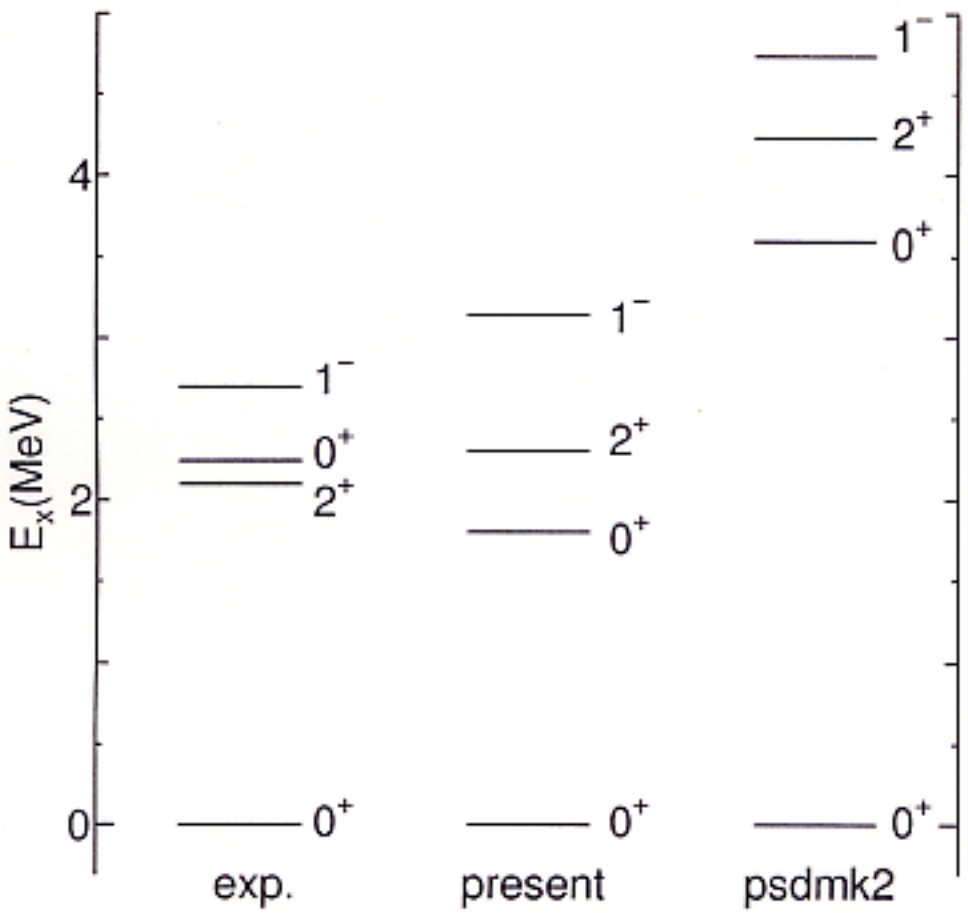

1^-, 0^+ > CNS exp.

Iwasaki et al. PLB 491, 8 (2000)

Shimoura et al. to be published.

outline

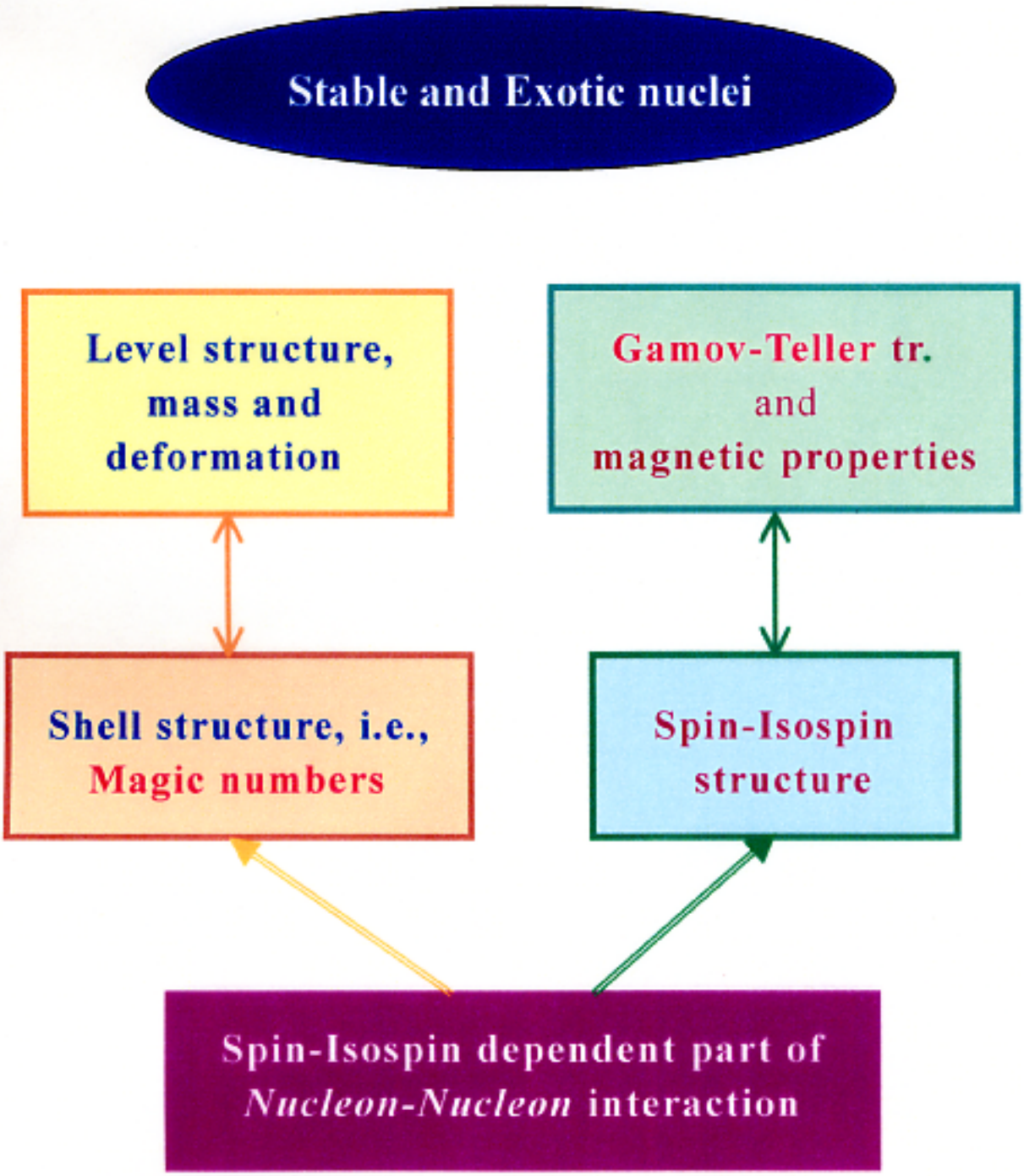
Stable and Exotic nuclei
Level structure, mass and deformation
Gamov-Teller tr. and magnetic properties
Shell structure, i.e., Magic numbers
Spin-Isospin structure
Spin-Isospin dependent part of *Nucleon-Nucleon* interaction

Magnetic moment of p-shell nuclei

$|\mu(\text{calc.}) - \mu(\text{exp.})|$

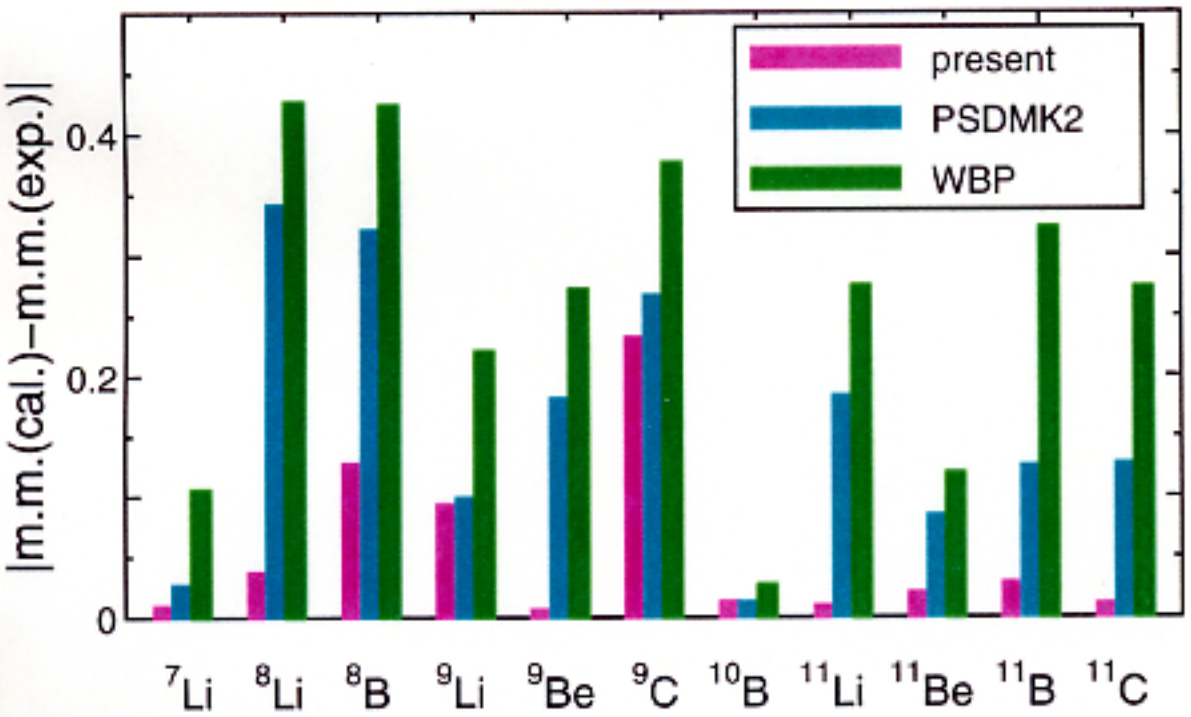

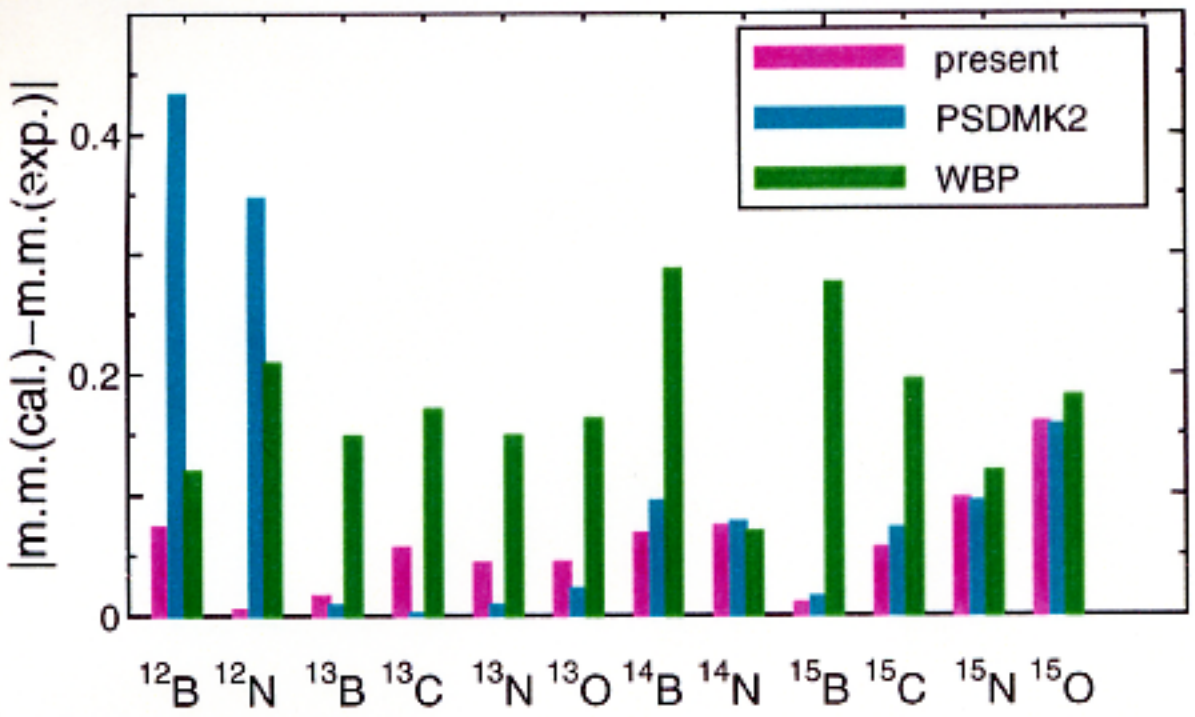

Summary

In some exotic nuclei, the magic numbers do change from those for stable nuclei.

stable	2,	8,	20,	28,	38 / 40,	…
exotic	2,	6,	16,	28,	34,	…

Origin : strong $j_> - j_<$ coupling in T=0 channel

as confirmed by G-matrix and empirical fit

A major basic mechanism producing this coupling :

$$(\tau\,\tau)\,(\sigma\,\sigma)\,f(r)$$

meson exchange and $1/N_c$ expansion of QCD

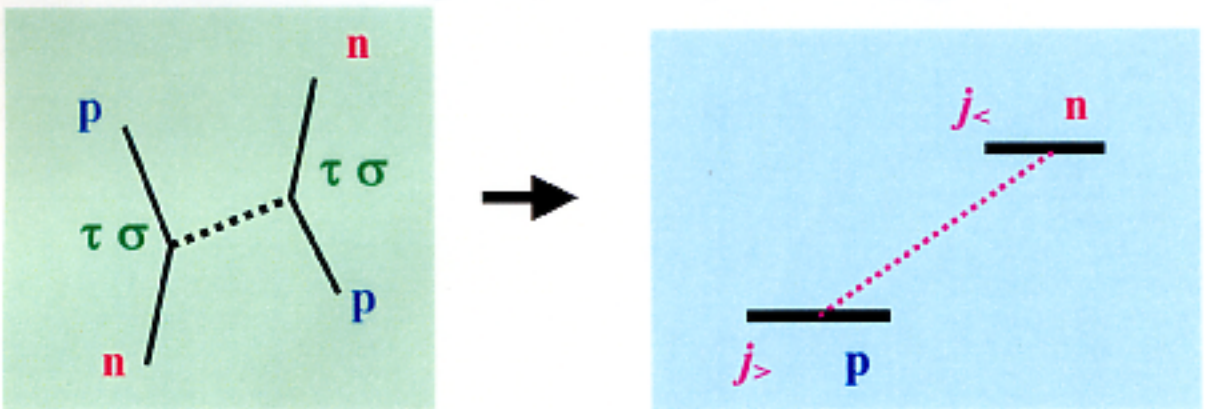

This explains various structures of exotic nuclei.

Paradigm of Shell Evolution

* * * * * * * * * * * * * *

The same interaction affects spin-isospin properties.

Magnetic moments, GT transitions, etc.

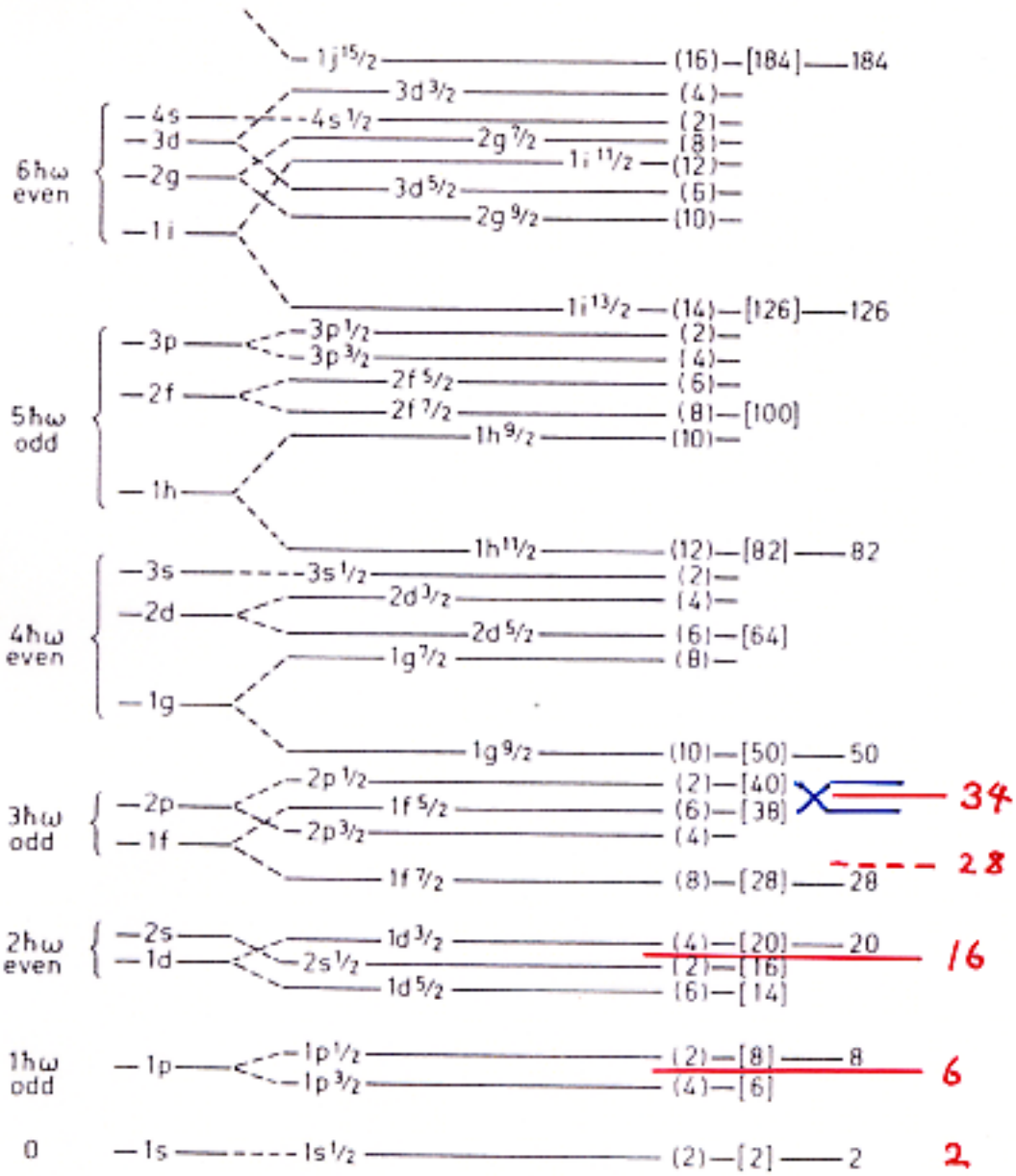

Figure 2-23 Sequence of one-particle orbits. The figure is taken from M. G. Mayer and J. H. D. Jensen, *Elementary Theory of Nuclear Shell Structure*, p. 58, Wiley, New York, 1955.

Magic Numbers in Exotic Nuclei and Spin-Isospin Properties of the *NN* Interaction

Takaharu Otsuka,[1,2] Rintaro Fujimoto,[1] Yutaka Utsuno,[3] B. Alex Brown,[4] Michio Honma,[5] and Takahiro Mizusaki[6]

[1]*Department of Physics, University of Tokyo, Hongo, Bunkyo-ku, Tokyo, 113-0033, Japan*
[2]*RIKEN, Hirosawa, Wako-shi, Saitama 351-0198, Japan*
[3]*Japan Atomic Energy Research Institute, Tokai, Ibaraki 319-1195, Japan*
[4]*National Superconducting Cyclotron Laboratory, Michigan State University, East Lansing, Michigan 48824*
[5]*Center for Mathematical Sciences, University of Aizu, Tsuruga, Ikki-machi, Aizu-Wakamatsu, Fukushima 965-8580, Japan*
[6]*Department of Law, Senshu University, Higashimita, Tama, Kawasaki, Kanagawa, 214-8580, Japan*

(Received 31 March 2001; published 3 August 2001)

The magic numbers in exotic nuclei are discussed, and their novel origin is shown to be the spin-isospin dependent part of the nucleon-nucleon interaction in nuclei. The importance and robustness of this mechanism is shown in terms of meson exchange, *G*-matrix, and QCD theories. In neutron-rich exotic nuclei, magic numbers such as $N = 8$, 20, etc. can disappear, while $N = 6$, 16, etc. arise, affecting the structure of the lightest exotic nuclei to nucleosynthesis of heavy elements.

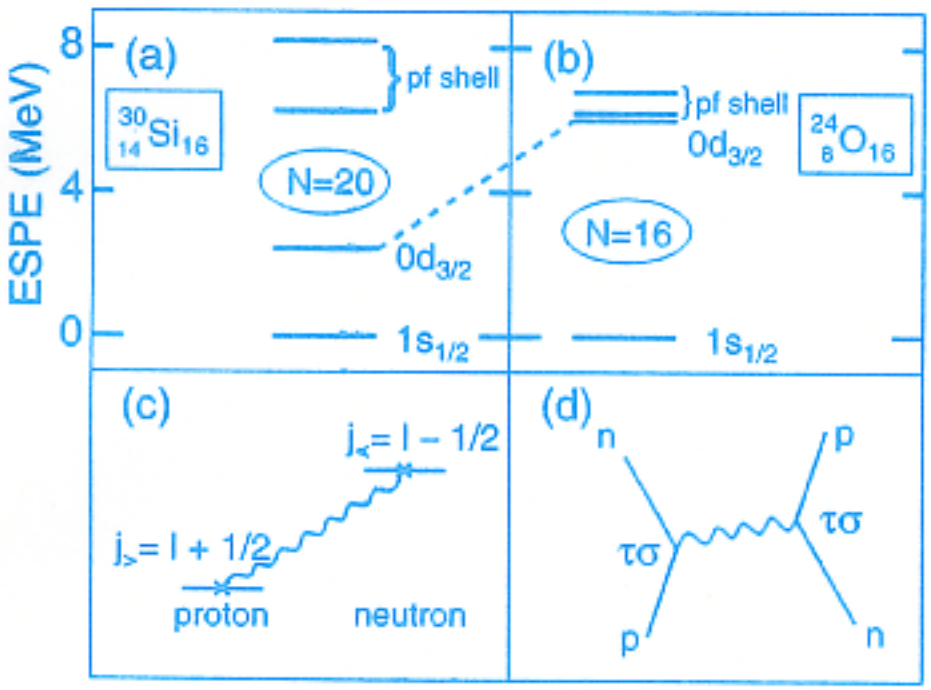

FIG. 1. Neutron ESPE's for (a) ^{30}Si and (b) ^{24}O, relative to $1s_{1/2}$. The dotted line connecting (a) and (b) is drawn to indicate the change of the $0d_{3/2}$ level. (c) The major interaction producing the basic change between (a) and (b). (d) The process relevant to the interaction in (c).